# THE STABILITY OF CLASSIFIED CRYSTALLIZERS

by

Gary Lee Beer

---

A Thesis Submitted to the Faculty of the

DEPARTMENT OF CHEMICAL ENGINEERING

In Partial Fulfillment of the Requirements
For the Degree of

MASTER OF SCIENCE

In the Graduate College

THE UNIVERSITY OF ARIZONA

1 9 7 3

## STATEMENT BY AUTHOR

This thesis has been submitted in partial fulfillment of requirements for an advanced degree at The University of Arizona and is deposited in the University Library to be made available to borrowers under rules of the Library.

Brief quotations from this thesis are allowable without special permission, provided that accurate acknowledgment of source is made. Requests for permission for extended quotation from or reproduction of this manuscript in whole or in part may be granted by the head of the major department or the Dean of the Graduate College when in his judgment the proposed use of the material is in the interests of scholarship. In all other instances, however, permission must be obtained from the author.

SIGNED: Gary Lee Beer

## APPROVAL BY THESIS DIRECTOR

This thesis has been approved on the date shown below:

Alan D. Randolph
Alan D. Randolph
Professor of Chemical Engineering

6/30/73
Date

## ACKNOWLEDGMENTS

The author wishes first to thank the director of this research, Dr. Alan D. Randolph, whose creative suggestion and patient review made this work possible. Dr. James P. Keener of the Mathematics Department of The University of Arizona is also gratefully remembered for his understanding aid in the analysis. Finally, the Department of Chemical Engineering of The University of Arizona and the National Science Foundation are acknowledged for providing the facilities and support required for this project.

TABLE OF CONTENTS

LIST OF ILLUSTRATIONS

LIST OF ILLUSTRATIONS--Continued

# ABSTRACT

The stability of CSD (crystal size distribution) for the R-z model of a classified product crystallizer with fines removal was studied by spectral analysis of the describing equation. The model included the possibility of magma-dependent nucleation rate and direct recycle of dissolved fines while assuming a high-yield, Class II, system. Fines removal and classification were described by various constant removal rates for each of the three size sections.

Stability limits were calculated in terms of dimensionless model parameters and presented as critical contours of the nucleation growth rate exponent, $i = d(\log B^0)/d(\log G)$. Magma-dependent nucleation was characterized by the solids concentration exponent in the kinetic expression. System specifics were lumped into the calculation of the steady state growth rate used to make the dimensionless analysis. The most influential parameters were found to be the classification size and the presence of fines recycle.

# INTRODUCTION

The desire to obtain a product or intermediate in a particular solid form often motivates the choice of crystallization as a unit operation. Besides producing a very high degree of separation, crystallization affords the designer some degree of control over the size and number of particles to be generated. The shape and purity can also be determined within certain limits; but the key measurement from which the acceptability of the output from an operating system may be judged depends upon the crystal size distribution (CSD). Thus there has been much emphasis placed upon the development of methods to predict and to produce satisfactory CSD. These efforts have modeled the crystallization process from a steady-state viewpoint, and the results assume that this point can be attained in practice. In fact, some such CSD outputs cannot be achieved in actual operation. Besides physical limits to the process, such as fouling of internal equipment due to excessive supersaturation levels, the most significant constraint on suitable behavior arises from the dynamics of the CSD. These variations can produce a variety of problems ranging from disturbance of a subsequent filtration operation to the inability to meet product specifications as to caking, habit, or size.

The actions of CSD in time can be divided into two categories, transients-caused and stability-linked responses. Transients appear as a result of time dependent influences on the system, such as a perturbation in flow rate or a change in feed concentration. Looking at transient behavior from the viewpoint of simulation, dynamics of this type are seen to follow time variant forcing functions on the describing set of differential equations. As the motivating disturbance dies, so eventually does the transient associated with it. Limit cycle behavior could possibly be explained by continual time-dependent forcing, but such disturbances should be apparent to operating personnel and thus be removable. Stability, on the other hand, does not depend on continuing activation from beyond the system. The unforced system structure determines stability limits, thus making stability a quality relatable only to the steady-state or design parameters of the system. Periodic cycling of CSD can be anticipated when values of the design variables are chosen, with unstable combinations of these variables being excluded. Existing systems may also be modified to remove the operation from a region of instability, but the necessary changes could be difficult or impossible to implement. In either situation quantitative action cannot be taken unless the location of stability limits in the parameter phase space can be predicted.

## BACKGROUND

In modeling crystallization processes, certain basic categorizations and techniques have been implemented. In the description of CSD, an average size, usually based upon weight, and a measure of deviation from this average, usually in the form of a coefficient of variation, are often used to characterize the output size distribution of a crystallizing system. These measures are calculable from a plot of accumulative particle weight as a function of a characteristic particle size. An acceptable model must therefore predict a distribution of particle sizes. To accomplish this, while accounting for CSD dynamics, the model must be distributed in both time and size.

Based upon the degree of supersaturation in the crystallizing suspension, two general types of system behavior are differentiated. A Class I system exhibits a measurable amount of supersaturation, while Class II systems maintain a high yield (i.e., $(C-C_s)/(C_i-C_s)$) even when CSD cycles. A Class II system may be thought of as a limiting case of Class I behavior. For either system the general procedure of model construction remains the same. First, a population balance is written based on the configurational arrangement of the crystallizer. Then nucleation kinetics, which appear in an end condition to the partial differential equation produced by the population balance, are formulated to describe the rate of formation of new particles at the smallest size suitable for growth. These nucleation expressions are often stated in powers of supersaturation or growth rate combined with solids concentration.

Several experiments have indicated secondary mechanism for nucleation as opposed to homogeneous, free volume dependent methods (Randolph 1971, p. 2). To complete the description, an over-all mass balance is written. This mass balance takes different forms depending on Class I or Class II behavior of the system; in systems of the latter type the mass balance becomes a constraint on crystal growth rate since the supersaturation becomes unmeasurable.

Through the mass balance, instability-creating feedback is introduced to the model. This feedback relationship is shown diagrammatically in Figure 1. For example, in a Class II system the mass balance becomes (Randolph and Larson 1971, p. 83)

$$G(t) = \frac{P_I(t)}{\frac{\rho V}{2} A(t)}, \tag{1}$$

where the total crystal area, A, is dependent upon CSD, and CSD in turn is a function of the linear growth rate, G.

In describing the residence time configuration for a crystallizer, the parameters chosen usually relate differences between the behavior to be modeled and that of the MSMPR (mixed suspension, mixed product removal) situation. Classification and fines removal may be looked upon as variations in removal rate over the size range in question when compared to the simple case of isokinetic removal from a well mixed suspension. Many industrial crystallizers utilize Class II systems (e.g., ammonium sulfate, potassium chloride, sodium chloride, etc.). If product size is large in such crystallizers, perhaps due to the utilization of a fines destruction system, then there is a good possibility for some product classification to occur due to non-isokinetic removal of the large-sized particles. Alternatively, deliberate product classification is implemented with classifying devices (e.g., wet screens, hydroclones, elutriators) in order to produce a narrower, more attractive distribution. Such process modifications as excessive fines destruction and/or product classification are reported to have resulted in unstable operation, i.e., a CSD that cycles.

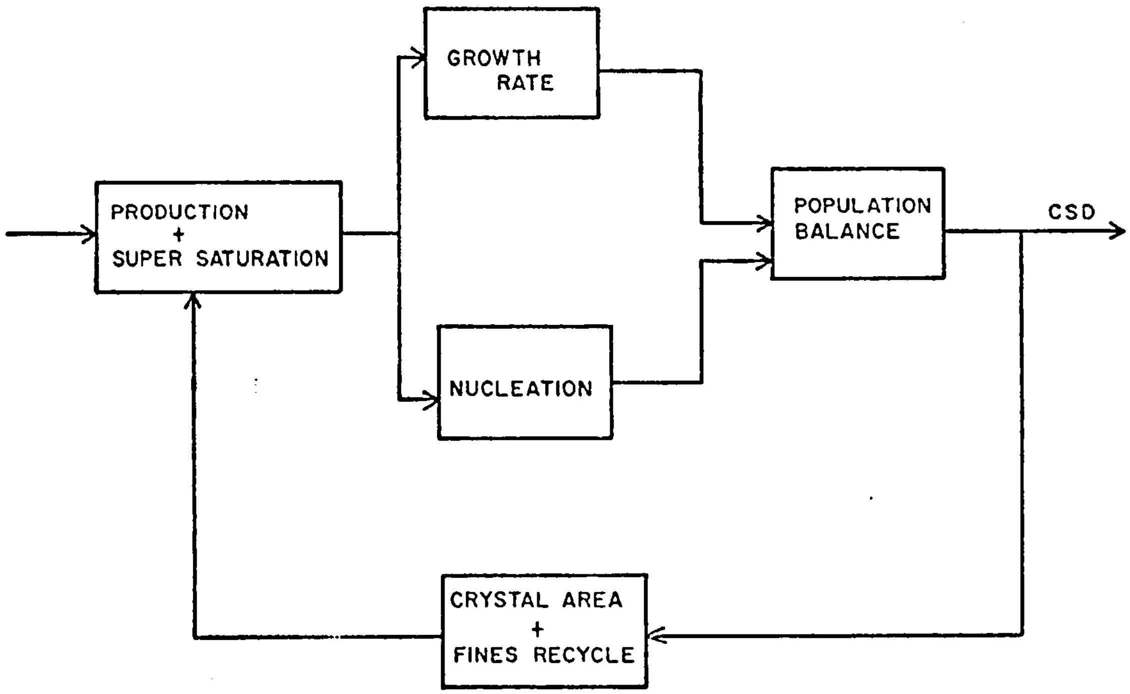


Fig. 1. Feedback Mechanism for Crystallization.

## PREVIOUS WORK

The earliest results pertaining to the stability of crystallization systems were those of Randolph (1964), who presented the relationship

$$\frac{d(\log B^0)}{d(\log G)} < 21 \qquad (2)$$

as the stability limit for an MSMPR crystallizer. This expression is not dependent upon the form of nucleation kinetics. Recent work in secondary nucleation kinetics indicates nucleation correlations of the form (Randolph and Cise 1971; Youngquist and Randolph 1972)

$$B^0 = k_N(\text{temperature, RPM})G^i M_T^j \qquad (3)$$

as being satisfactory to fit the majority of data from MSMPR crystallizers. Since solids concentration does not vary in a Class II MSMPR, the criterion of Eq. (2) yields the fact that i, from Eq. (3), must be less than 21 for stable operation of this system. This limit is well above reported values of i, which fall almost exclusively below 10. Thus cycling of CSD in an MSMPR crystallizer cannot be expected unless supersaturation levels are driven to regions of discontinuity in nucleation rate (Figure 2). In other words, no unstable MSMPR systems can exist in the supersaturation region described by secondary nucleation. Stability limits obtained by Randolph and Larson (1971, p. 231) assuming nucleation was correlated with various moments of the CSD instead of solids concentration are as follows:

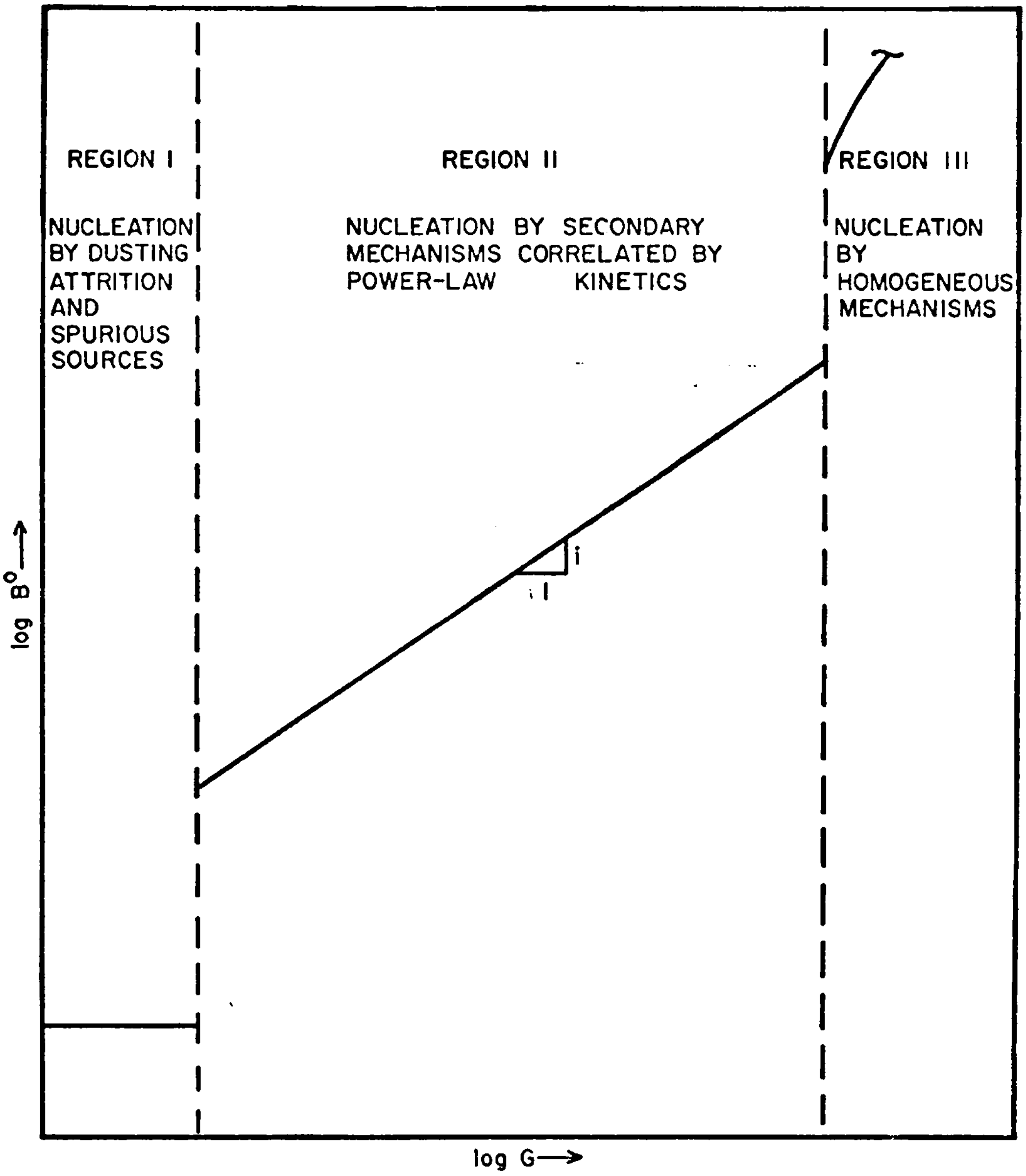


Fig. 2. Hypothetical Plot of Nucleation Rate vs Supersaturation Driving Force (after Randolph 1971).

For $B^0 = k_N G^i M_1{}^j$,

$$i < 21 - 2j. \tag{4}$$

For $B^0 = k_N G^i M_4{}^j$,

$$i^2 - 7i + 25j < 294. \tag{5}$$

No significant change in the $i < 21$ criterion can be noted for these Class II results for reasonable values of the parameter j.

Sherwin, Shinnar, and Katz (1969) describe the dynamics of an ideally classified crystallizer with no product drawoff up to a size $L_p$ and instantaneous removal thereafter. Figure 3 shows the number density distribution with these assumptions. Nucleation rate was assumed to be independent of solids concentration. Total nucleation rate in this model was a function of void fraction and hence the stability regions were defined on this basis as well as the nucleation/growth rate kinetics. The onset of unstable response was predicted to occur at values of i as low as 2 for reasonable void fraction levels. This study demonstrated the strong effect that differences in particle residence time can have on stability limits. That is, extreme classification could lower the nucleation sensitivity stability limit to the range of realistic nucleation/growth rate kinetics.

Hulburt and Stefango (1969) studied CSD dynamics in a double-drawoff crystallizer. Such crystallizers, having a mixed suspension underflow and an overflow of particles smaller than size $L_f$, are used to increase both particle size and solids concentration. The double-drawoff crystallizer can be said to advance fines (Fig. 4, p. 13) from the system

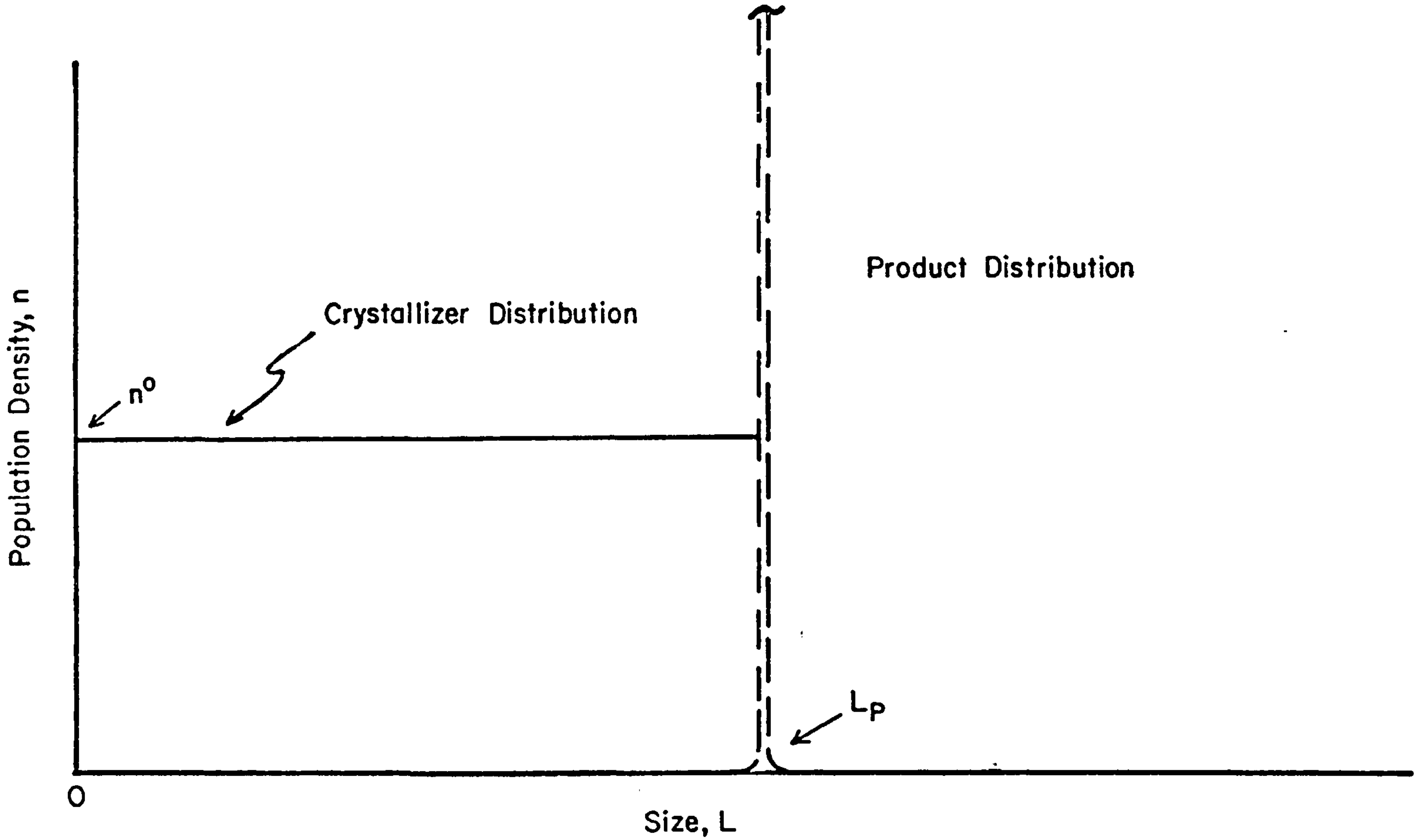


Idealized Classification Model (after Sherwin, Shinnar & Katz)

Fig. 3. Number Density vs Size Curve for Idealized Classification.

rather than to destroy them. A nucleation-growth rate model yielding both Class I and, in the limit of rapid growth, Class II behavior was considered. A weak dependency was found for nucleation/growth rate sensitivity on clear liquor overflow rate and on the maximum size of particle advanced. A limit of

$$\frac{d(\log B^0)}{d(\log G)} \simeq 20 \rightarrow 30 \tag{6}$$

was necessary for unstable CSD in the limit of Class II behavior. The nucleation/growth rate stability parameter passed through a minimum as the system was taken from extreme Class I behavior to the Class II high yield limit. However, even with the lowest calculated stability limits, low-order CSD cycling cannot be explained by this model.

Lei, Shinnar, and Katz (1971a) presented a stability analysis of a mixed suspension crystallizer with a finite fines trap. They employed a model similar to the one used in the above work. Stability limits were found to first increase, then decrease as the maximum size of fines removed went up for a given fraction of nuclei surviving. For a "point" fines trap, in which particles are removed at very small sizes, the modified MSMPR Class II stability limit, $i < 21 - \lambda$, was demonstrated. In this model, $e^{-\lambda}$ is the fraction of original nuclei surviving the fines trap. Again, low-order cycling of CSD cannot be accounted for based on the model and configuration analyzed.

Lei, Shinnar, and Katz (1971b) apply the stability analysis above to the control of a fines removing crystallizer. Direct feedback control of such systems is not possible until a method of on-the-spot sampling of small particle populations can be introduced to practice.

The above references all approach the problem in a similar manner. A lumped solute mass balance is written together with a distributed population balance and an equation for nucleation kinetics. The solute balance becomes a constraint on growth rate for Class II systems. The population balance is then linearized, and stability is examined by spectral analysis. Alternatively (for the MSMPR cases) a moment transformation may be used to convert the partial differential equation of the population balance into a set of ordinary differential equations. This set is then linearized together with the mass balance constraint, and classical linear stability analysis is applied to predict stability limits.

## SCOPE

Three process configurations currently available in commercial crystallization machines are fines destruction, classified product removal, and clear liquor advance. Fines removal may occur either from a trap or through the top of a shielded settling area. The fines are then destroyed by heating and recycled directly to the mixed suspension. Product classification can be externally imposed (e.g., wet screens, elutriators) or inadvertently occurs in a mixed magma vessel due to settling or non-isokinetic product removal. Product size increases brought about by fines destruction may also increase classification of the larger particles at the point of removal; this reduces the size improvement expected from theoretical considerations. The net result is that a narrower, more attractive CSD may be produced, but the problem of cycling is intensified. CSD modification is sometimes limited by stability.

Randolph and Larson (1971, ch. 8) discuss the so-called R-z crystallizer model shown in Figure 4. In this model fines are removed, dissolved, and recycled, in sizes from nuclei to $L_f$, at R-1 times the MSMPR rate, while product, in the sizes above $L_p$, is removed at z times the MSMPR rate. Clear liquor may be advanced to increase solids concentration. The idealized R-z model can describe such condition configurations; fines removal, classification, and clear liquor advance represent the current state of the art in crystallization technology.

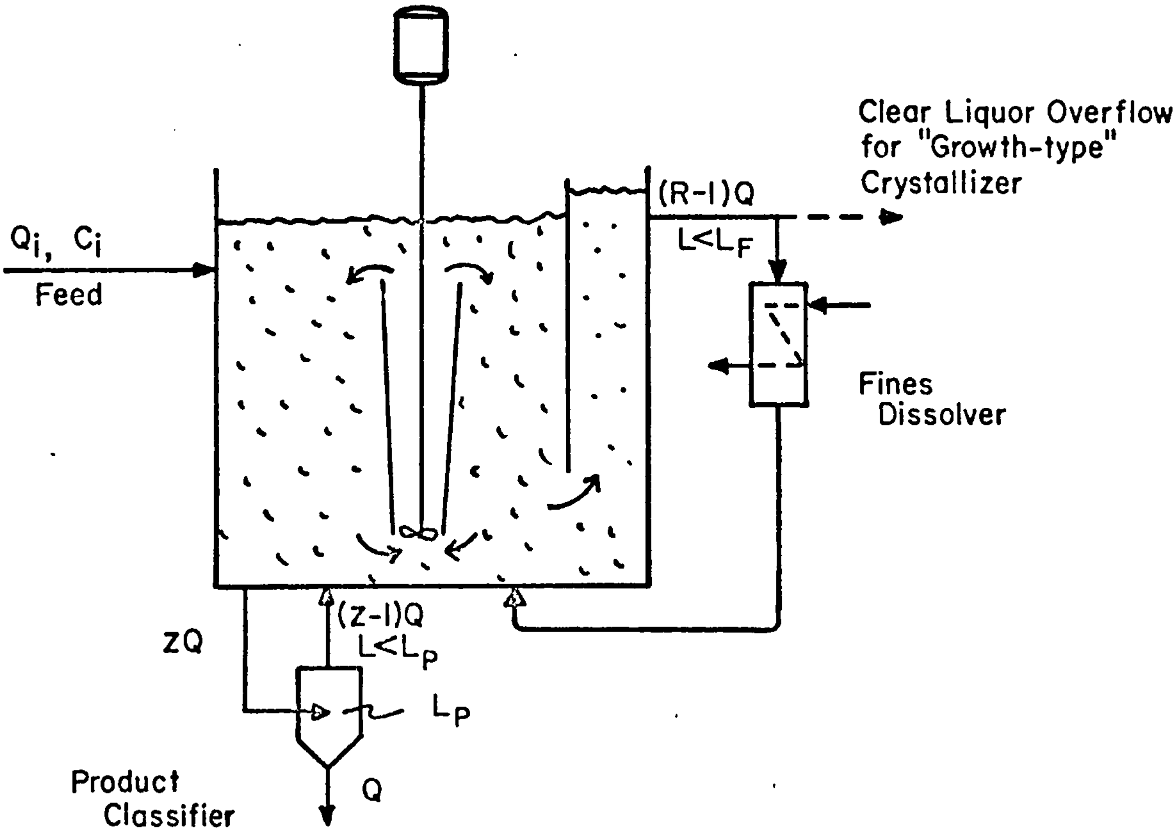


Fig. 4. Idealized Model of R-z Fines Dissolver/Classified Product Crystallizer.

The Class II, R-z, steady-state CSD equations lend themselves to an analytic, though complex, solution. The normalized population distribution for this model is (Randolph and Larson 1971, ch. 8)

$$x_f = L_f/G\tau \qquad x_p = L_p/G\tau \qquad y = n/n^0$$

$$\begin{aligned} Y_1 &= \exp(-Rx), & 0 \le x \le x_f \\ Y_2 &= \exp[-(R-1)x_f]\cdot\exp(-x), & x_f \le x \le x_p \\ Y_3 &= \exp[-(R-1)x_f + (z-1)x_p]\cdot\exp(-zx), & x \le x_p. \end{aligned} \tag{7}$$

Figure 5 plots this dimensionless population density. The mass balance evolves into a growth rate constraint which, if nucleation kinetics of Eq. (3) are assumed, is given by (Appendix A)

$$G = \left(\frac{P_E}{6D_pQ}\right)^{\frac{1-j}{i+3}} \left(6D\right)^{\frac{-j}{i+3}} \left(\rho k_V k_N \tau^4\right)^{\frac{-1}{i+3}} \tag{8}$$

where

$$D_p = \frac{w(Rx_f)}{R^4} + \exp[-(R-1)x_f]\cdot[w(x_p) - w(x_f)] + \exp[(z-1)x_p - (R-1)x_f]\cdot[1 - w(zx_p)]/z^3$$

$$D = \frac{w(Rx_f)}{R^4} + \exp[-(R-1)x_f]\cdot[w(x_p) - w(x_f)] + \exp[(z-1)x_p - (R-1)x_f]\cdot[1 - w(zx_p)]/z^4$$

$$w(p) = \frac{1}{6}\int_0^p x^3 e^{-x} dx = 1 - \exp(-p)(1 + p + p^2/2 + p^3/6).$$

Equation (8) gives G as an implicit functionality, and the solution must be iterative. This value of growth rate is equivalent to the balance set

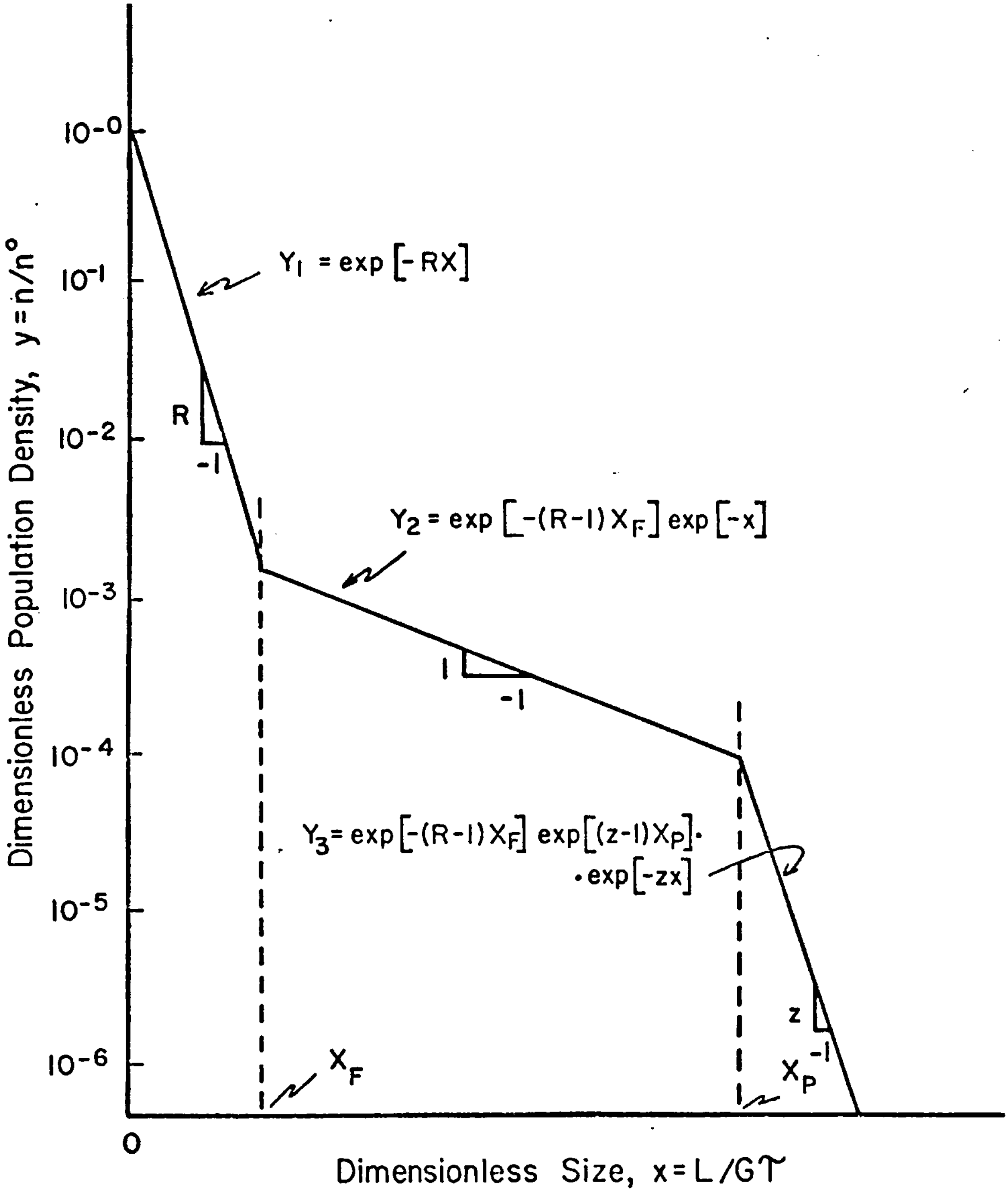


Fig. 5. Steady-State Population Distribution for the Idealized Crystallizer.

forth in Eq. (1); the external production constraint forces growth rate to high enough values to compensate for additional internal rate of make as fines are dissolved and recycled. If fines are advanced, then their mass must be subtracted from $P_E$, thus lowering the required growth rate.

The R-z model derives from the algorithm of simultaneous solution of mass and population balances taken together with system nucleation kinetics and an idealized process configuration. The power law kinetics used here may depend explicitly on the solids concentration but not upon void fraction. Using the above model, the aim is to evaluate the stability limits of Class II classified crystallizers with a fines dissolver. Realistic magma-dependent nucleation is assumed, and fines recycle is anticipated. Results are presented in the framework of the R-z model parameterization.

## DEVELOPMENT OF EQUATIONS

The generalized population balance presented by Randolph (1964) may be written for a well mixed suspension as

$$\frac{\partial n}{\partial t} + \nabla \cdot \underline{V_i} n + n \frac{d \log V}{dt} = B - D - \sum_k Q_k n_k / V. \tag{9}$$

Now, if the following assumptions are made

1. Constant crystallizer volume, V
2. Isothermal, self-seeded operation
3. Equal specific volume for feed and exit streams
4. Thin slurry density ($d \log V/dt \simeq 0$)
5. Negligible breakage and agglomeration (birth function $B \to 0$ and death function $D \to 0$)
6. Crystal size as the internal coordinate ($\nabla \cdot \underline{V_i} n = \partial Gn/\partial L$)

the balance becomes

$$\frac{\partial n}{\partial t} + \frac{\partial (Gn)}{\partial L} = - \sum_k n_k Q_k / V. \tag{10}$$

The application of McCabe's $\Delta L$ law yields $[G \neq G(L)]$

$$\frac{\partial n}{\partial t} + G \frac{\partial n}{\partial L} = - \sum_k n_k Q_k / V. \tag{11}$$

For the R-z model the last term may be written as

$$- \sum_k n_k Q_k / V = -h(L) n / \tau \tag{12}$$

where

$$h(L) = R, \quad 0 \le L \le L_f$$
$$h(L) = 1, \quad L_f < L \le L_p$$
$$h(L) = z, \quad L_p < L.$$

The population balance for the dynamic R-z model may thus be presented as

$$\frac{\partial n}{\partial t} + G\frac{\partial n}{\partial L} + h(L)n/\tau = 0. \tag{13}$$

Using the assumptions made in deriving the population balance, a dynamic material balance may be made. This balance can be derived from either general total solute balances (e.g., Hulbert and Katz 1964, see Appendix B) or equating the generation of new solids to the disappearance of solute. Making this latter balance gives

$$\sum Q_i C_i - QC - V\rho k_a \int_0^\infty \frac{G}{2} n\, L^2\, dL = 0 \tag{14}$$

or, with $G \neq G(L)$,

$$G = 2\left[\frac{\sum Q_i C_i}{Q} - C\right] \Bigg/ \left(\tau\rho k_a \int_0^\infty n\, L^2\, dL\right) \tag{15}$$

or

$$G = \frac{P_I(t)}{\frac{\rho V}{2} A(t)} . \tag{16}$$

Now the term $P_I$ contains any recycle of fines. The expression may be better written in terms of the external production rate $P_E$ plus the mass of fines recycled:

$$P_I = P_E + (R-1)\, Q\, \rho k_V \int_0^{L_f} n\, L^3\, dL. \tag{17}$$

The over-all dynamic mass balance then becomes

$$G = \frac{P_E + (R-1)\, Q\, \rho\, k_V \int_0^{L_f} n\, L^3\, dL}{\frac{\rho V}{2}\, k_a \int_0^{\infty} n\, L^2\, dL} \tag{18}$$

or, eliminating $k_a$ by means of $k_V = k_a/6$,

$$G = \frac{P_E + (R-1)\, Q\, \rho\, k_V \int_0^{L_f} n\, L^3\, dL}{3\rho V k_V \int_0^{\infty} n\, L^2\, dL} . \tag{19}$$

$P_E$ as given by Randolph and Larson (1971, p. 145) is

$$P_E = \rho k_V \int_0^{\infty} Q(L)\, n\, L^3\, dL \tag{20}$$

or

$$P_E = 6\rho\, k_V\, n^0 (G\tau)^4\, Q\, D_p . \tag{21}$$

Finally, after some simplification, the dynamic mass balance becomes for the R-z model

$$G = \frac{6n^0 (G\tau)^4 D_p + (R-1) \int_0^{L_f} n\, L^3\, dL}{3\tau \int_0^{\infty} n\, L^2\, dL} . \tag{22}$$

Nucleation kinetics assumed the form

$$B^0 = k_N\, G^i\, M_T{}^j \tag{23}$$

or

$$B^0 = n^0 G = k_N G^i (\rho k_V \int_0^{\infty} n\, L^3\, dL)^j . \tag{24}$$

The complete set of model equations may be collected as

$$\frac{\partial n}{\partial t} + G\frac{\partial n}{\partial L} + h(L)n/\tau = 0 \tag{25}$$

$$n(0,t) = \frac{B^0}{G} = k_N G^{i-1} (\rho k_V \int_0^\infty n L^3 dL)^j$$

$$G = [6n^0(G\tau)^4 D_p + (R-1)\int_0^{L_f} n L^3 dL] / (3\tau \int_0^\infty n L^2 dL)$$

$$n(L,0) = \bar{n}(L) \qquad \text{(R-z steady-state solution).}$$

Now making the dimensionless transformation of Eq. (25) by means of

$$y = \frac{n}{n_0{}^0}, \quad x = \frac{L}{G_0\tau}, \quad \phi = \frac{G}{G_0}, \quad \theta = t/\tau, \tag{26}$$

with $n_0{}^0$ being the steady-state number density of nuclei and $G_0$ being the steady-state growth rate, we obtain

$$\frac{\partial y}{\partial \theta} + \phi\frac{\partial y}{\partial x} + h(x)y = 0 \tag{27}$$

$$y(0,\theta) = \phi^{i-1} (\int_0^\infty x^3 y\, dx / \int_0^\infty x^3 \bar{y}\, dx)^j$$

$$y(x,0) = \bar{y}\ [\text{Eq. (7)}]$$

$$\phi = \frac{6D_p + (R-1)\int_0^{x_f} x^3 y\, dx}{\int_0^\infty x^2 y\, dx} \cdot \frac{\int_0^\infty x^2 \bar{y}\, dx}{6D_p + (R-1)\int_0^{x_f} x^3 \bar{y}\, dx}.$$

The moments are normalized by ratio to their steady-state values as

$$f_2 = \frac{\int_0^\infty x^2\, y\, dx}{\int_0^\infty x^2\, \bar{y}\, dx}, \quad f_3 = \frac{\int_0^\infty x^3\, y\, dx}{\int_0^\infty x^3\, \bar{y}\, dx}, \quad f_{3,1} = \frac{\int_0^{x_f} x^3\, y\, dx}{\int_0^{x_f} x^3\, \bar{y}\, dx}$$

$$\beta = \frac{(R-1)}{6D_p} \int_0^{x_f} x^3\, \bar{y}\, dx. \tag{28}$$

Finally, using Eqs. (28), we write the set of dimensionless, normalized equations for the dynamic R-z model

$$\begin{aligned} \frac{\partial y}{\partial \theta} + \phi \frac{\partial y}{\partial x} + hy &= 0 \\ y(0,\theta) &= f_3{}^j\, \phi^{i-1} \\ y(x,0) &= \bar{y} \\ \phi &= \frac{1+\beta f_{3,1}}{1+\beta} \cdot \frac{1}{f_2} \end{aligned} \tag{29}$$

Linearization was made by perturbation expansion about the steady state (Appendix C), giving the set

$$\begin{aligned} \frac{\partial \tilde{y}}{\partial \theta} + \frac{\beta}{1+\beta} h\bar{y}\, \tilde{f}_{3,1} + h\, \bar{y}\, \tilde{f}_2 + \frac{\partial \tilde{y}}{\partial x} + h\tilde{y} &= 0 \\ \tilde{y}(0,\theta) &= j\tilde{f}_3 + \frac{(i-1)}{1+\beta} \beta\, f_{3,1} - (i-1)\tilde{f}_2 \\ \tilde{y}(x,0) &= 0. \end{aligned} \tag{30}$$

This set presents the linearized dynamics of an R-z crystallizer with removal configuration h(x), magma dependent nucleation through j, and including fines dissolving and recycle characterized by β as defined earlier.

Stability criteria may be extracted from Eq. (30) by spectral techniques which parallel those used by Lei et al. (1971a). This spectral analysis is based on examination of all solutions of Eqs. (30) under the transform $\partial\tilde{y}/\partial\theta = s\tilde{y}$. The conclusion of the analysis is a matrix equation of the form (Appendix D)

$$\underline{\underline{A}} \times \underline{\underline{F}} = \underline{\underline{0}}. \tag{31}$$

The complete description of the terms in Eq. (31) is given by Figure 6. The characteristic equation is found by expanding det(A) by minors and setting it equal to zero (see Appendix E). Thus, the characteristic equation is

$$Y_\infty^{\ 3} Y_{x_f}^{\ 3}\left[(i-1)H_\infty^{\ 2} + G_\infty^{\ 2} + Y_\infty^{\ 2}\right] - \frac{\beta}{1+\beta} Y_\infty^{\ 2} Y_\infty^{\ 3}\left[(i-1)H_{x_f}^{\ 3} + G_{x_f}^{\ 3}\right]$$
$$- j\, Y_\infty^2 Y_{x_f}^3 H_\infty^3 - j\, Y_{x_f}^{\ 3}\begin{vmatrix} G_\infty^2 & H_\infty^2 \\ G_\infty^3 & H_\infty^3 \end{vmatrix} + j\,\frac{\beta}{1+\beta} Y_\infty^{\ 2}\begin{vmatrix} H_\infty^2 & G_\infty^2 \\ H_{x_f}^{\ 3} & G_{x_f}^{\ 3} \end{vmatrix} = 0. \tag{32}$$

This equation is linear in (i-1) and may be written

$$i-1 = \psi(H_\alpha^{\ n}, G_\alpha^{\ n}, Y_\alpha^{\ n}, j, \beta, s) \tag{33}$$

## CLASS II CRYSTALLIZER INTEGRAL EQUATIONS OF LINEARIZED SET

$$\begin{pmatrix} (i-1)H^2_\infty + G^2_\infty + Y^2_\infty & \left(\frac{i-1}{1+\beta}\right)\beta\, H^2_\infty + \left(\frac{\beta}{1+\beta}\right)G^2_\infty & j\, H^2_\infty \\ (i-1)H^3_\infty + G^3_\infty & \left(\frac{i-1}{1+\beta}\right)\beta\, H^3_\infty + \frac{\beta}{1+\beta}\, G^3_\infty & j\, H^3_\infty - y^3_\infty \\ (i-1)H^3_{x_F} + G^3_{x_F} & \frac{(i-1)}{1+\beta}\beta\, H^3_{x_F} + \frac{\beta}{1+\beta}\, G^3_{x_F} - y^3_{x_F} & j\, H^3_{x_F} \end{pmatrix} \begin{pmatrix} -F_2 \\ F_{3,1} \\ F_3 \end{pmatrix} = 0$$

WHERE

$$H^n_\alpha = \int_0^\alpha x^n\, H(x)dx \qquad H(x) = \exp[sx - \int_0^x h(\tau)d\tau\ ]$$

$$G^n_\alpha = \int_0^\alpha x^n\, G(x)H(x)dx \qquad G(x) = \int_0^x h(\tau)e^{-s\tau}d\tau$$

$$Y^n_\alpha = \int_0^\alpha x^n\, \bar{y}dx \qquad \bar{y}(x) = \text{steady-state R-z distribution}$$

Characteristic Equation $\det(A(s)) = 0$

Fig. 6. Matrix Form of the Characteristic Equation.

where $\psi$ is the function given in Appendix E. Now i-1 is real but $\psi$ is complex, so

$$i = \mathrm{Re}(\psi) + 1.0 \qquad (34)$$
$$0 = \mathrm{Im}(\psi).$$

If the spectral variable s on the threshold of instability is taken as a purely imaginary number ($s = 0 + b\sqrt{-1}$), then

$$\begin{aligned} i &= \mathrm{Re}[\psi(b)] + 1 \\ 0 &= \mathrm{Im}[\psi(b)] \end{aligned} \qquad (35)$$

for a given point in the parameter space. A Fortran IV program was written to locate roots of $\mathrm{Im}[\psi(b)]$, and values of i at these roots were used to define the limit of stable operation. For example, for a chosen set of design, operating, and system parameters (excluding i), the program locates the value of i at which cycling begins to occur. Systems exhibiting higher values of i result in unstable operation, and lower values result in stable operation. A flow chart of the computer algorithm is shown in Figure 7.

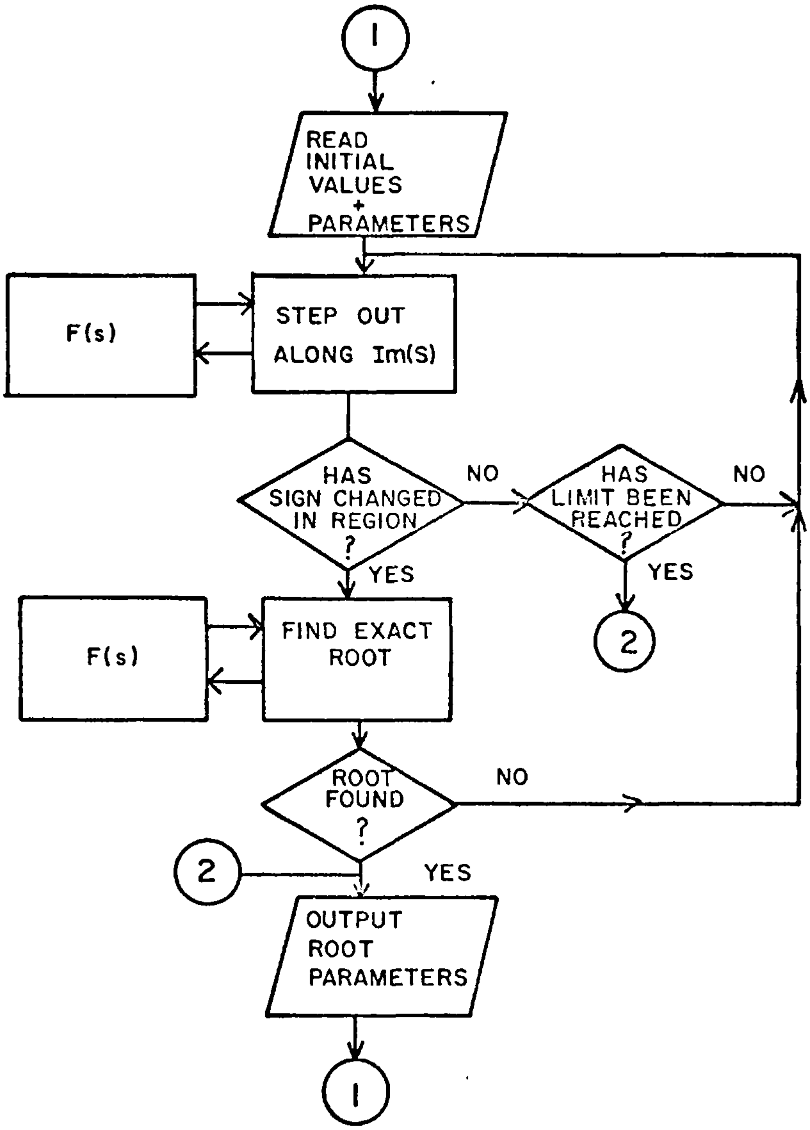


Fig. 7. Flow Chart of Computer Algorithm.

## STABILITY RESULTS

By first examining each parameter set in the R-z model separately (e.g., z and $x_p$) and then in combination, the interactions of the entire model can be more easily evaluated. The effects of fines recycle and magma-dependent nucleation rates will be developed in parallel.

### Fines Removal

The first results presented deal with the problem of fines removal only. The characteristic equation for $j = 0$ and $\beta = 0$ becomes

$$(i-1)H_\infty^2 + G_\infty^2 + Y_\infty^2 = 0. \tag{36}$$

This may be compared to the results of Lei et al. (1971a), which when taken to the limit of Class II behavior give as the characteristic equation

$$(i-1)H_\infty^3 + G_\infty^3 = 0 \tag{37}$$

with h(x) for both Eq. (36) and Eq. (37) defined as

$$\begin{aligned} h &= R, \qquad x \le x_f \\ h &= 1 \qquad\; x > x_f. \end{aligned} \tag{38}$$

The differences in characteristic equations are due to the inclusion of void fraction in the nucleation rate expression for the model of Eq. (37). The results for the only region of comparison ($j = 0$, no recycle) are presented in Figure 8. Both models predict a point fines stability limit of $21 - \lambda$. The destruction of a significant mass of fines in the absence

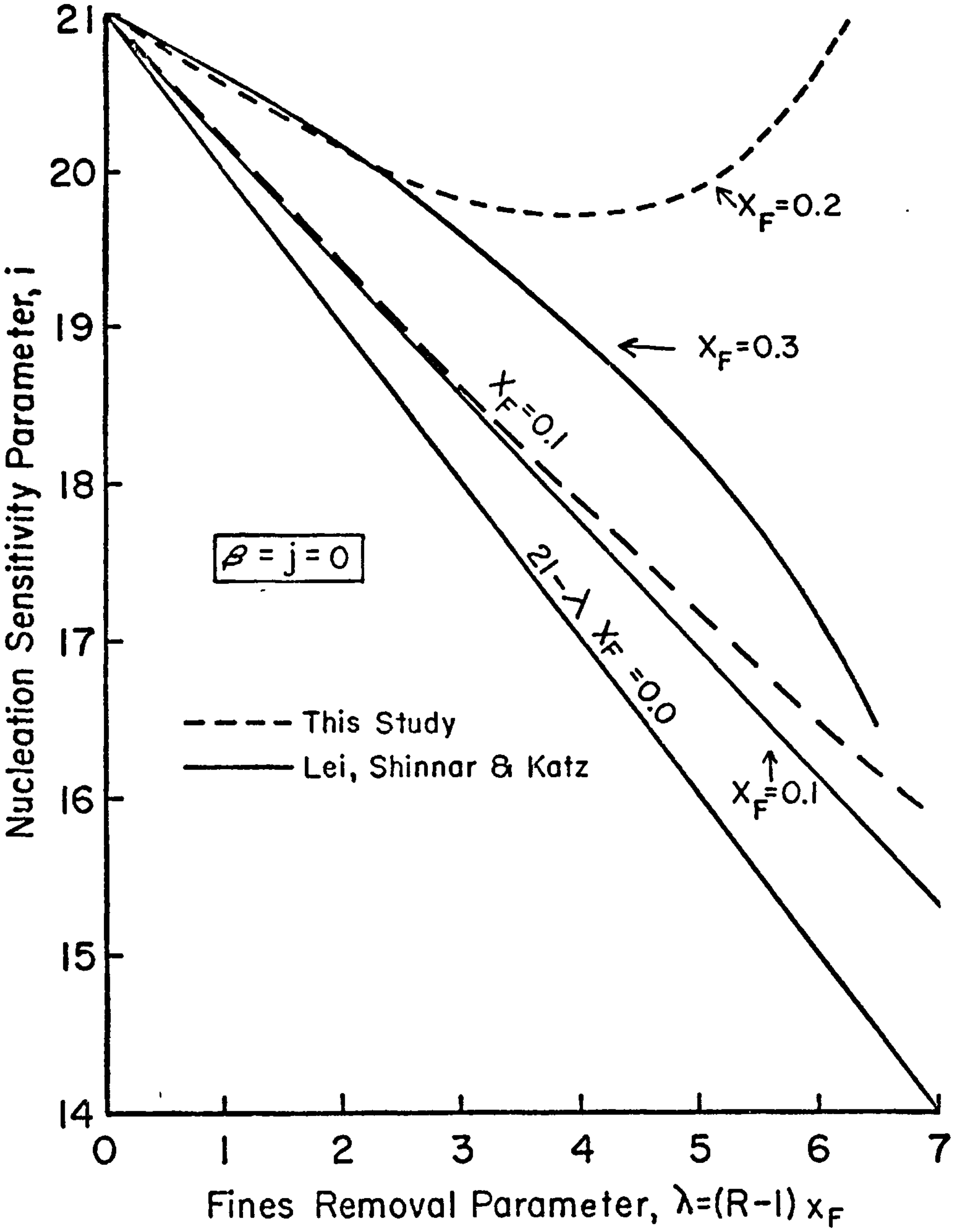


Fig. 8. Effect of Fines Removal on CSD Stability.

of any recycle tends to stabilize CSD for the R-z model, since results for $x_f > 0$ all lie above the point fines removal limit and the stable region is enlarged. Figure 9, when compared to Figure 8, demonstrates the dramatic effect of recycling fines mass. As fines size increases, the stability limit i passes through a minimum for reasonable values of $\lambda$; this may be best observed in Figure 10. Note that, for a large fines removal size, CSD is totally stabilized. The inclusion of various values of solids dependency in the nucleation rate, given by the parameter j, produced negligibly different results for both the recycle and nonrecycle cases. This result is entirely expected in the case of recycled fines, as the dissolved fines are immediately converted to an equivalent mass, grown over the entire distribution by the rapid Class II kinetics; solids concentration is therefore not perturbed.

The point fines case, for the combinations considered thus far, remains the most destabilizing situation save for some extreme values of $\lambda$. However, fines removal alone lowers the stability limit only to the range 14-20 and fails to account for low-order cycling of CSD.

## Classification

Figure 11 demonstrates the strong effect of classification on CSD stability. The stability parameter i falls rapidly with z for removal values up to approximately 4. The curves all saturate for high values of z (above 6) to a reasonably constant value of i. For small dimensionless classification sizes $x_p$ and high relative removal rate z, the stability sensitivity parameter i can be brought lower than 5. Figure 12 shows the dependence of i on $x_p$. The critical range for low values of i can be seen as extending down from $x_p$ sizes below 4.

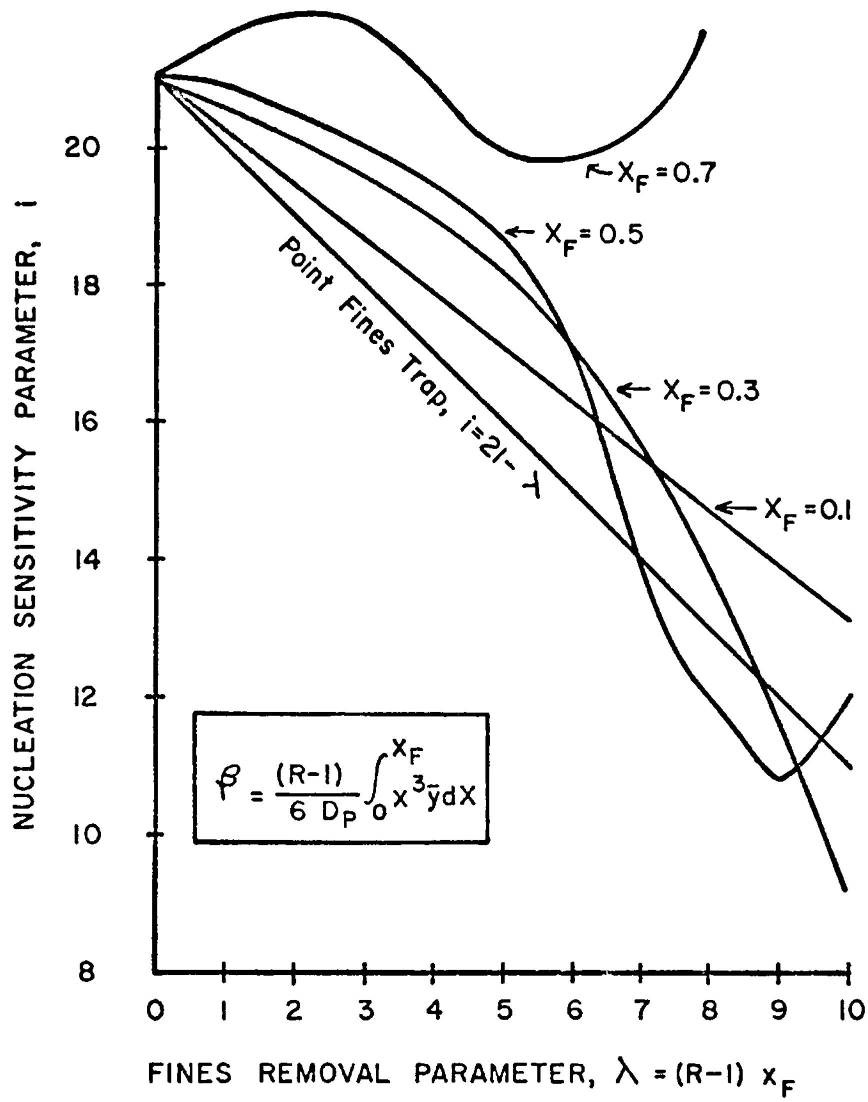


Fig. 9. Effect of Fines Removal on CSD Stability:
Recycle of Dissolved Fines.

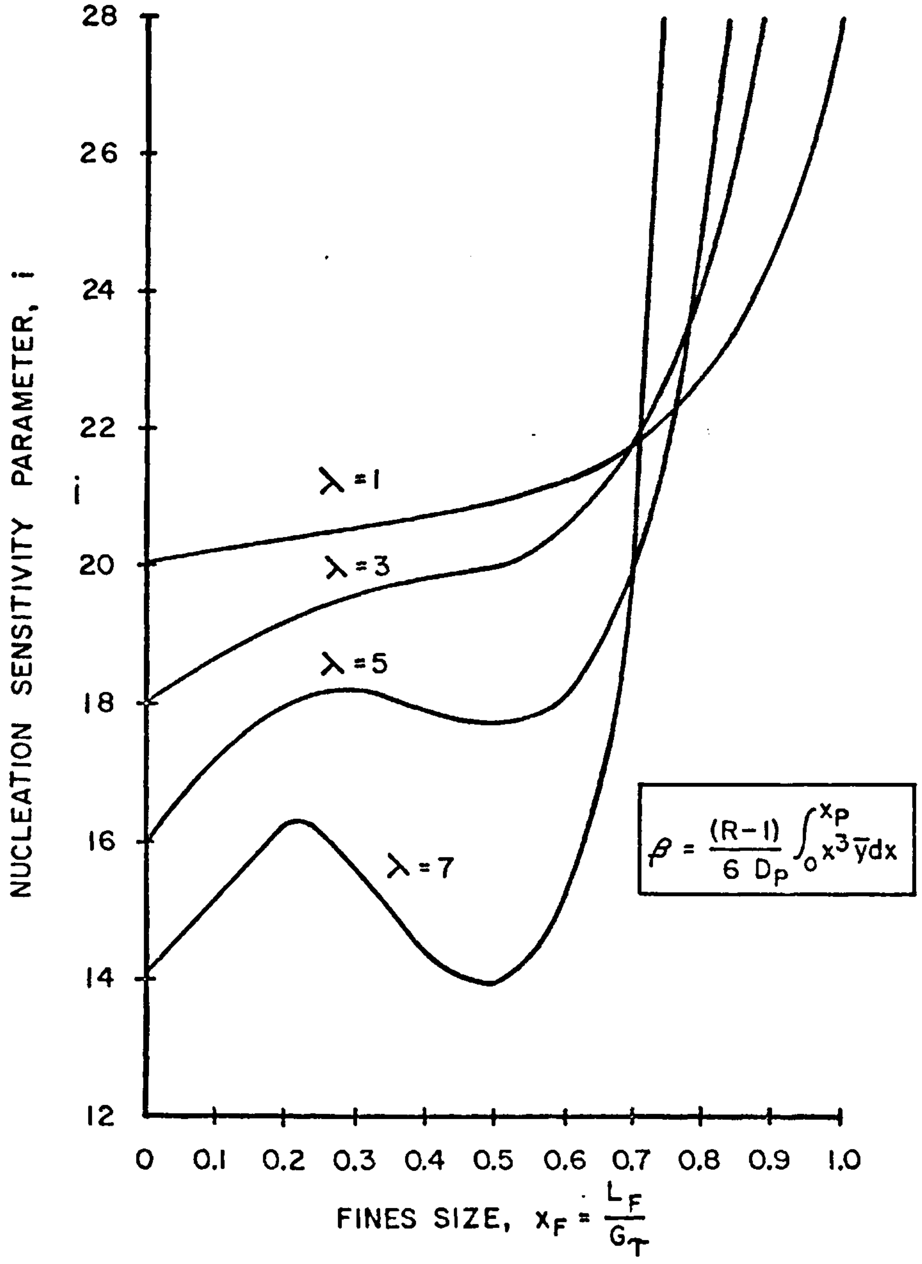


Fig. 10. Effect of Fines Size on CSD Stability.

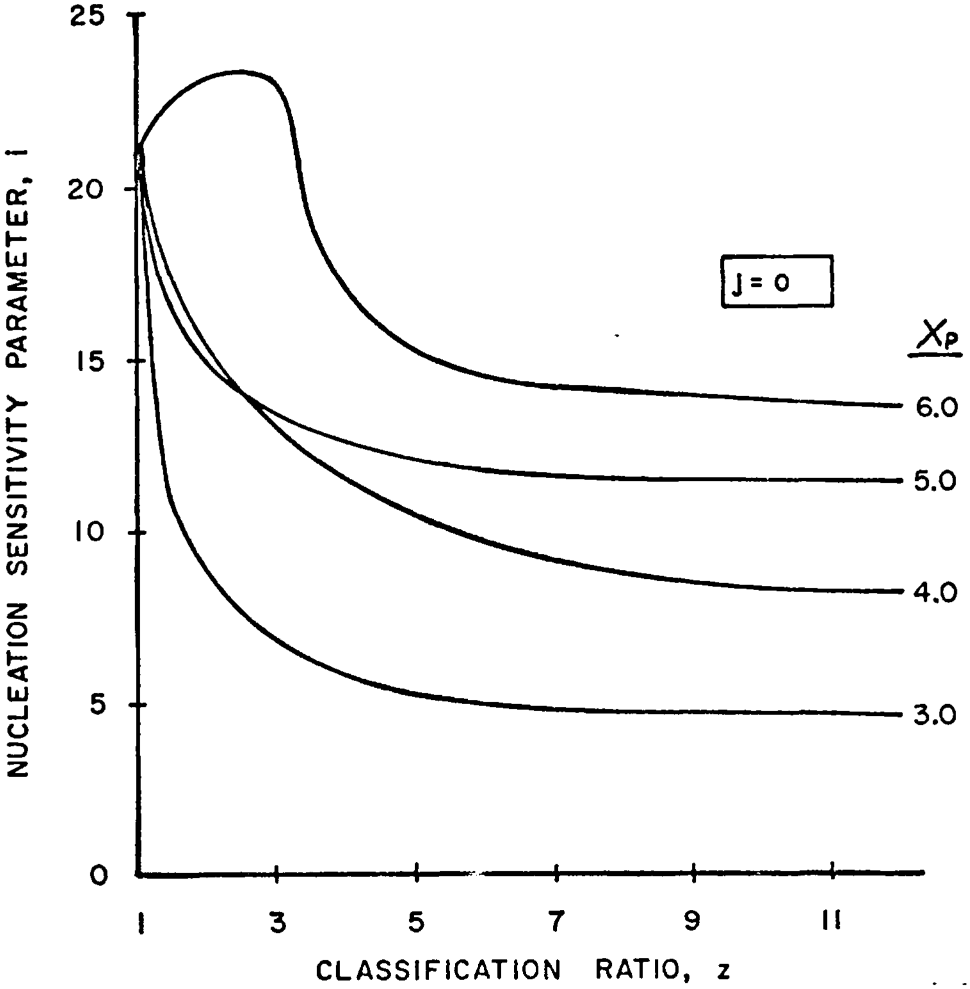


Fig. 11. Effect of Product Classification on CSD Stability.

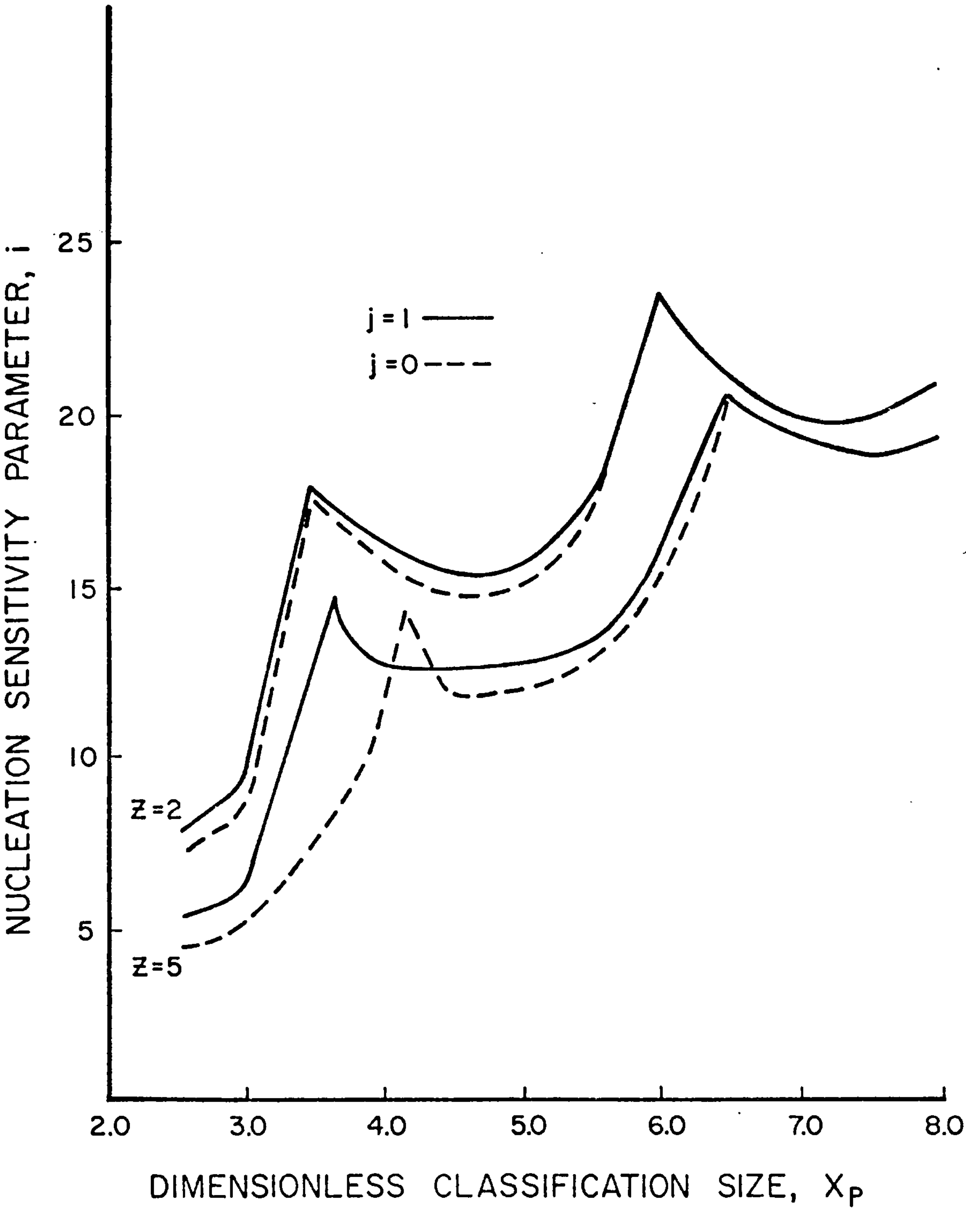


Fig. 12. Effect of Product Classification on CSD Stability: Magma-Dependent Nucleation.

The effect of magma dependency in the nucleation expression on classification-induced stability limits is superimposed on Figure 12 for $j = 1$. A slight stabilizing effect can be noted, disappearing as $x_p$ increases. As the classification size goes up, the deviation from MSMPR conditions and stability decreases. As $x_p$ becomes very large (greater than 10), MSMPR behavior is exhibited and i approximates 21 for all z and j.

## Fines Removal with Classification

The combined effects of fines removal and of product classification are shown in Figure 13 for the cases where no internal recycle of fines occurs. Owing to the strong stabilizing effect of fines removal at $x_f$ sizes larger than about 0.2 (see Figure 8), only the calculations for $x_f = 0.1$ are presented. Low values of i can be observed in Figure 13 for $x_p = 3$. Thus product classification with fines removal at small sizes could explain low-order CSD cycling that has been reported in commercial crystallization machines. Note that the curves are nearly linear and qualitatively similar to the $x_f = 0.1$ curve shown in Figure 8 for fines destruction only.

Figure 14 uses the same axes and parameters as Figure 10, with the added effect of classification described by $x_p = 4$ and $z = 7$. The curves of constant $\lambda$ exhibit analogous behavior for the classified and unclassified cases. The curves of Figure 14 asymptote toward complete stabilization at higher values of $x_f$ for the same level of the survival parameter $\lambda$. Classification does not change the qualitative appearance of the curves but does produce a major quantitative shift in the

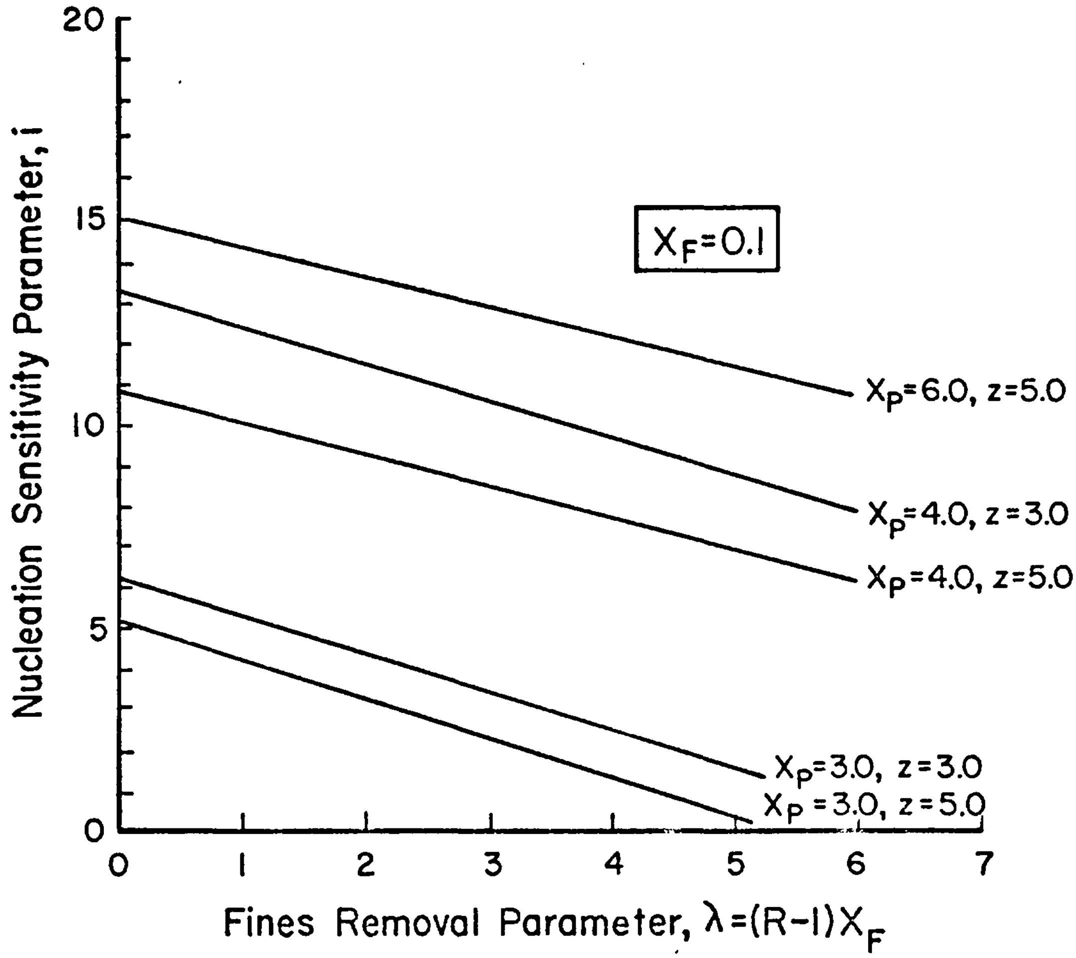


Fig. 13. Crystallizer Stability vs Dissolving Parameter $\lambda$ for Various Amounts of Product Classification.

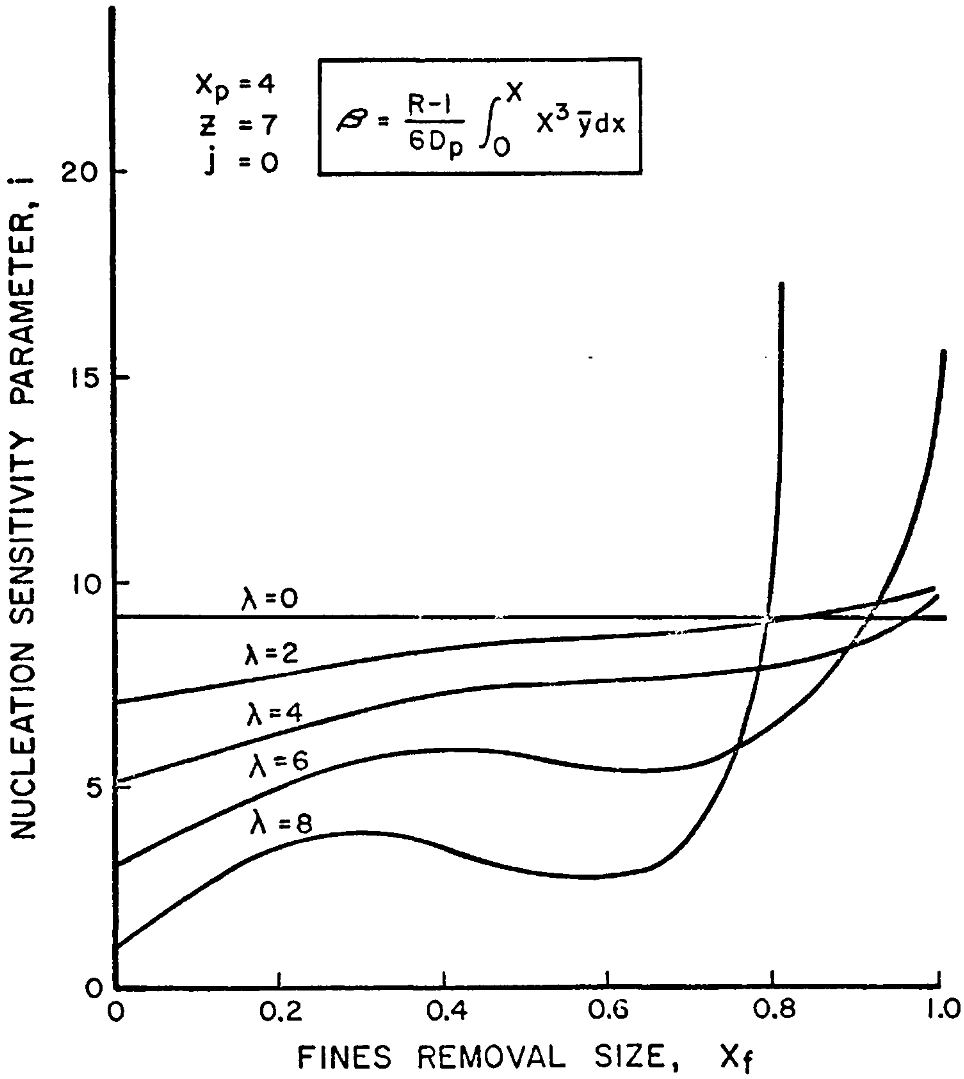


Fig. 14. Crystallizer Stability vs Fines Removal Size at a Certain Classification Rate and Size ($x_p = 4$, $z = 7$).

stability limits. The most significant effects of classification are the gross lowering of the stable limit and the requirement of larger sizes of fines removal size to achieve stabilization. These two characteristics make possible low-order CSD instability over narrow ranges of $\lambda$, z, $x_f$, and $x_p$.

Figure 15 demonstrates the effect of magma-dependent nucleation kinetics upon stability. The general result is an increase of the value of i necessary for the onset of instability at a given point in the parameter space. This stabilization diminishes as $\lambda$ increases (low orders of i), making the effect of magma-dependent nucleation minimal in the region of predicted low-order CSD cycling. The curves of constant maximum fines size $x_f$ in Figure 15 behave similarly to those of Figure 9 (no classification) except for the shifting on the stability axis due to classification.

A more complete picture of the stability limits may be gathered from Figures 16 and 17. These present various values of the classification size as parameters on curves representative of the fines removal stability behavior. Classified removal rate was at a high enough value to reflect the saturated limits displayed in Figure 11. The magma dependent nucleation parameter j was incremented by 1.0 to produce the two graphs shown. Thus, for the most realistic model used, low-order CSD cycling again requires that $x_p$ be less than 4 for a high rate of classified removal and reasonably attainable fines destruction. For example, at a dimensionless classification size of 3, the value of 8 may be reduced to less than 3 with values of $\lambda$ in the interval from 3 to 7.

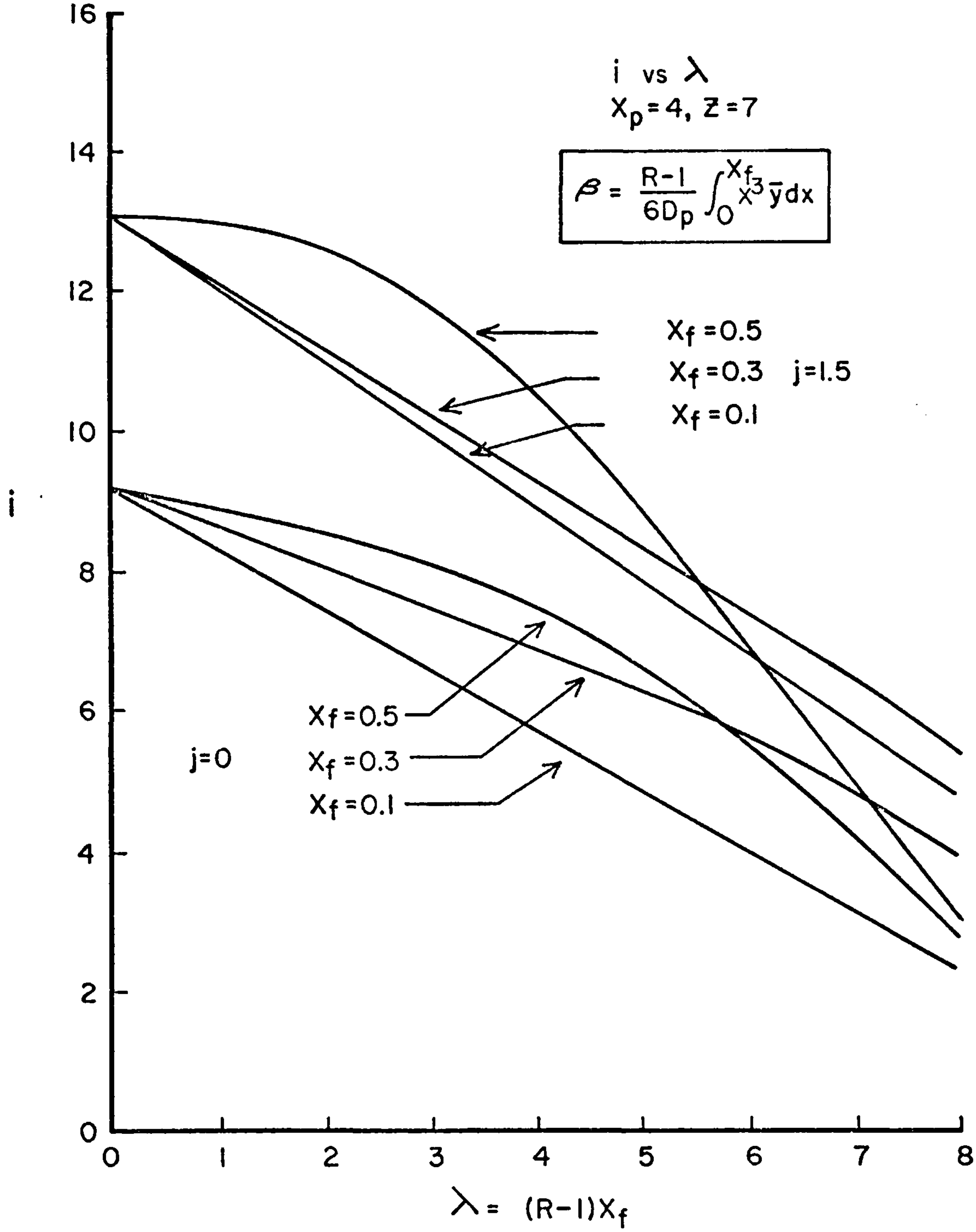


Fig. 15. Effect of Magma-Dependent Nucleation Rate on Classified Stability Limits.

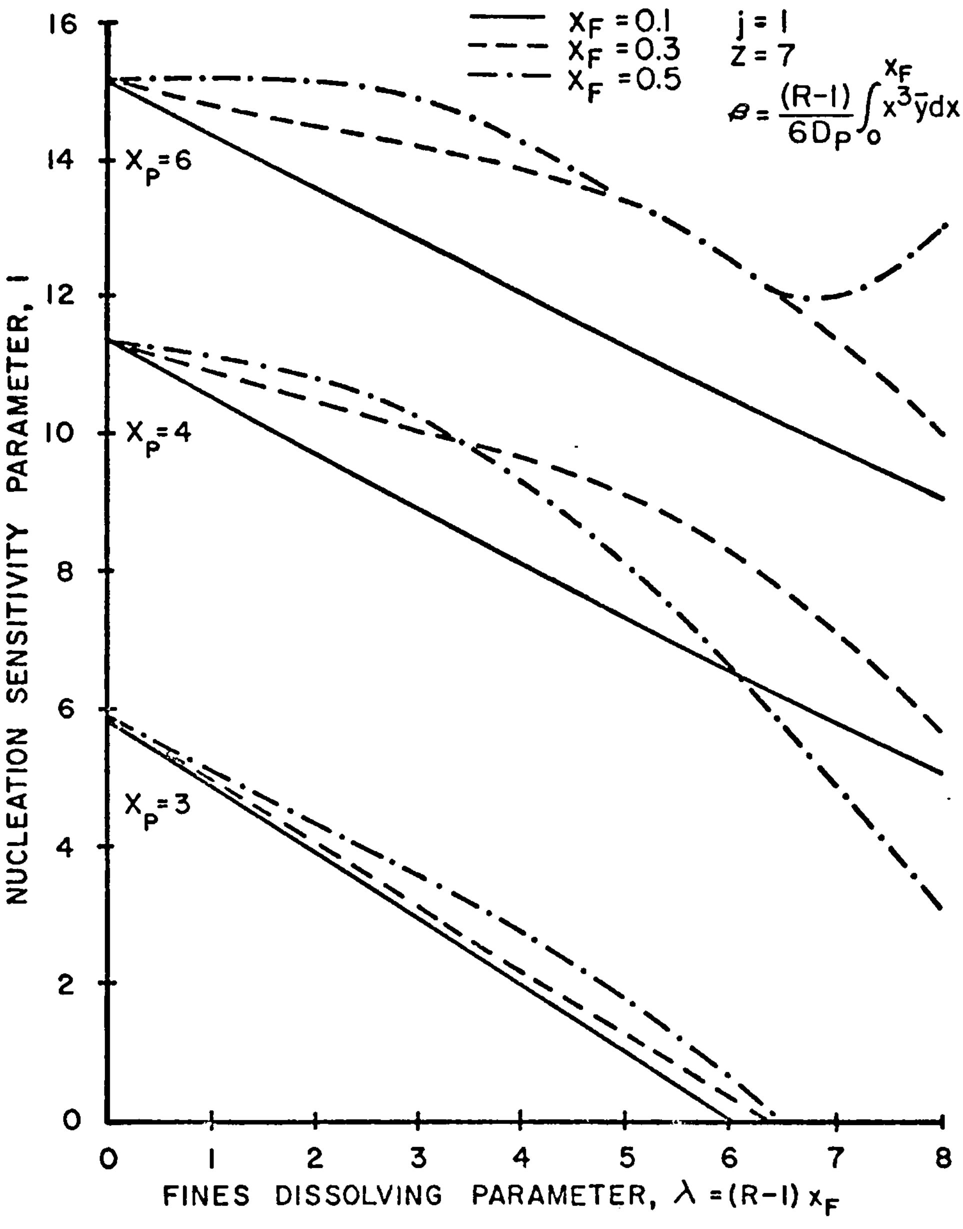


Fig. 16. Crystallizer Stability for the R-z Crystallizer with Fines Distribution and Classified Product Removal (Magma-Independent Nucleation).

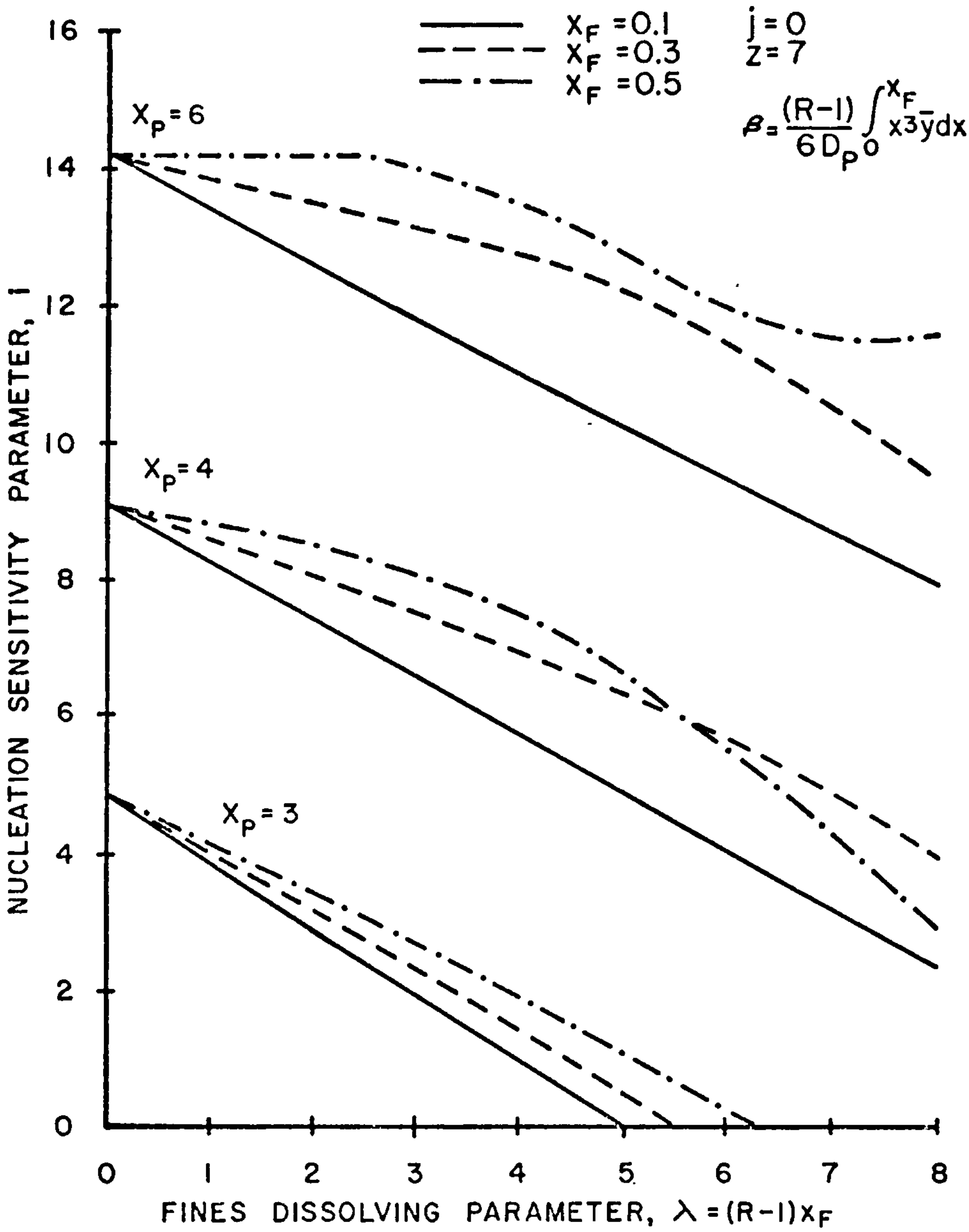


Fig. 17. Crystallizer Stability for the R-z Crystallizer with Fines Distribution and Classified Product Removal (Magma-Dependent Nucleation).

## Steady-State Results

The above results are presented in terms of the dimensionless parameters $\lambda$, $x_f$, $z$, $x_p$, and $j$. The behavior of the parameters $x_f$ and $x_p$ with alterations in process configuration are vital to an understanding of the stability limits presented. The quantitative basis of the dimensionless size parameters is the solution of the steady-state growth rate constraint. $G_0$ depends upon $P_E$, $Q$, $V$, $L_f$, $L_p$, $k_N$, $i$, $j$, $k_V$, and $\rho$ [see Eq. (8)]; in other words, $G_0$ is system dependent. Any generalized presentation of $G_0$ would have to be in terms of all system parameters and would not be of much practical use.

An important measure of CSD is the weight-averaged size of both the particles in suspension and those reporting to product. These values can be calculated, for a given configuration, as ratios of the fourth to the third moments of the respective distributions. The dimensionless average sizes in the product and in suspension are shown in Figure 18 for various classification sizes with no fines removal. The values of the weight-averaged size in the product are larger than those in suspension as expected with product classification. The averaged size in the product is smaller than the classification size for high values of $z$ and all reasonable sizes of $x_p$. In Figure 19 the ratio of the weight averaged product size to classification size is presented as a function of classification size with a strong removal rate $z$ and with no fines destruction. The possibility of low-order cycling appears at $x_p$ less than four. Thus, from Figure 19, instability may be possible if the product average size becomes more than 80% of the classification size.

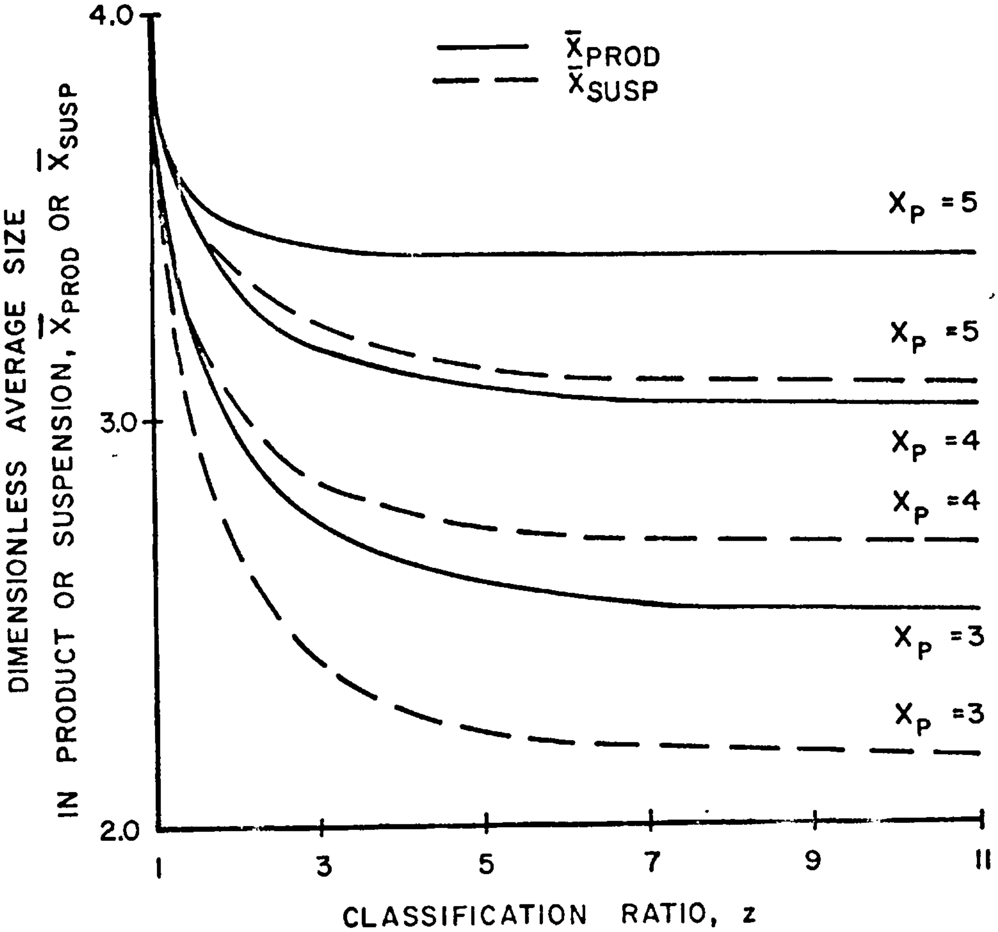


Fig. 18. Effect of Product Classification on Mean Particle Size.

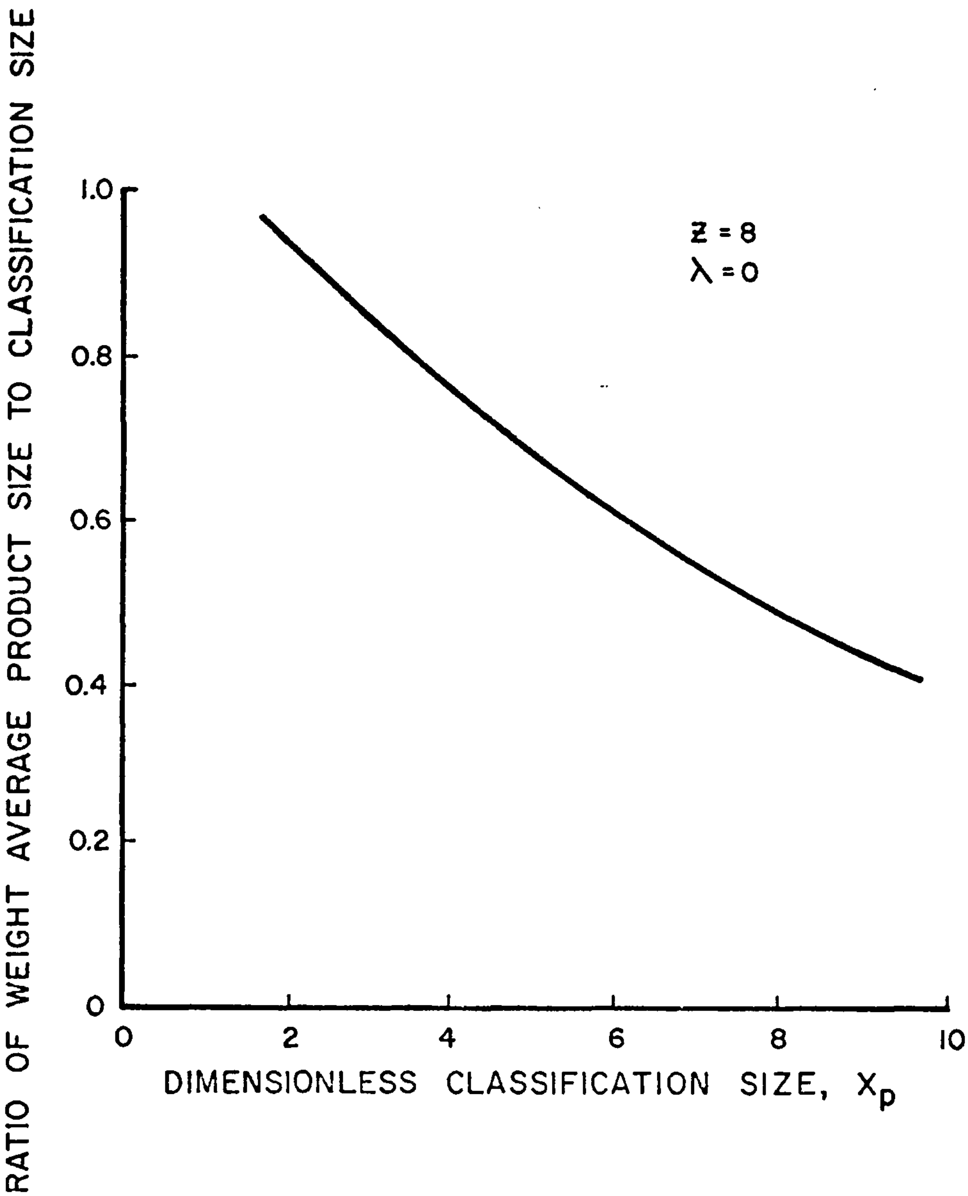


Fig. 19. Ratio of Weight-Averaged Product Size to Classification Size, vs Classification Size.

Another measure that can be calculated from dimensionless arguments is the ratio of the dissolver mass flow to the total internal production rate. This value, denoted as $\beta/(1+\beta)$, appears in the characteristic equation for recycle and is plotted as a function of the fines removal parameters in Figure 20 with no classification present. A practical upper limit for this ratio is about 0.3, which includes a wide range of $\lambda$ and $x_f$ combinations. The situation is of course complicated by the presence of classification. Figure 21 presents the behavior of both the weight-averaged size of product and the ratio of dissolver mass flow to internal make rate as functions of the fines removal parameters, for a given classification scheme. $\overline{X}_{prod}$ remains relatively unaffected by fines removal and recycle up to the aforementioned 0.3 limit. The $\lambda$ and $x_f$ combinations that fall below this limit have been shifted owing to the presence of classification. Classification raises the magnitude of $\beta/(1+\beta)$ by reducing the number of larger particles in the CSD.

## Verification of Results

In order to verify the stability analysis and to examine the behavior of the steady-state growth rate with configurational changes, a Class II simulation case study by Nuttall (1971) is considered. The system used kinetics of the form

$$B^0 = 3.2 \times 10^{33} G^6 \tag{39}$$

where G is in cm/sec. The production rate was kept at about 2.77 g/sec. The flow rate through the crystallizer was 16.7 $cm^3$/sec for a holding time of 1200 sec, and $\rho k_V$ was set equal to 2.13 $g/cm^3$.

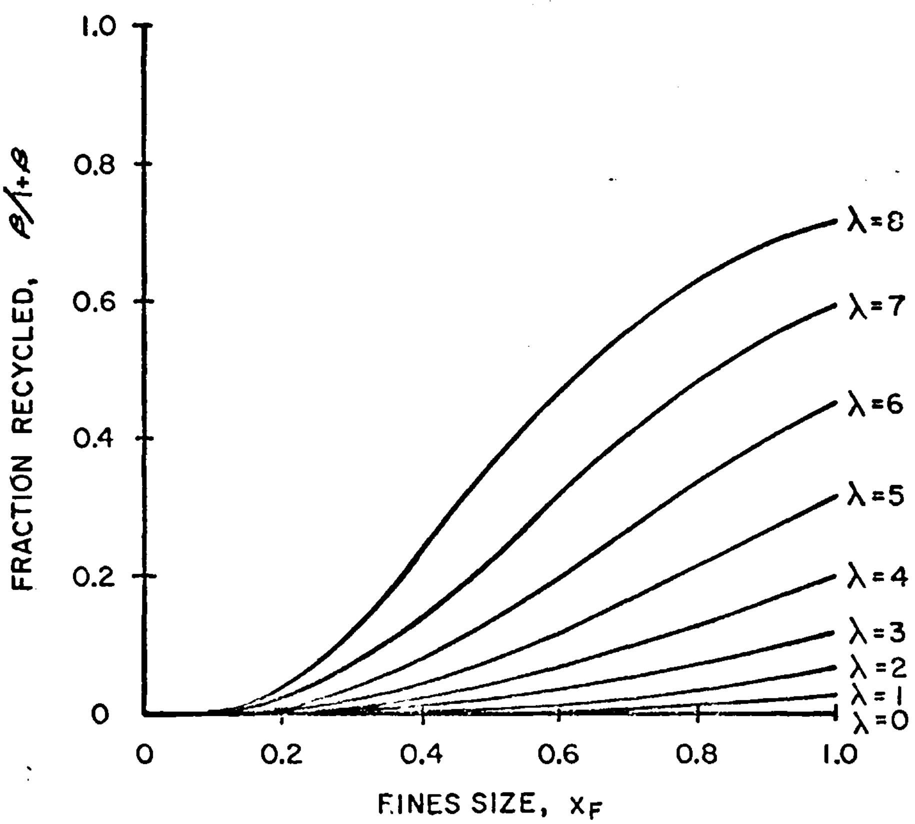


Fig. 20. Fraction of Total Internal Make Rate Due to Recycle of Dissolved Fines.

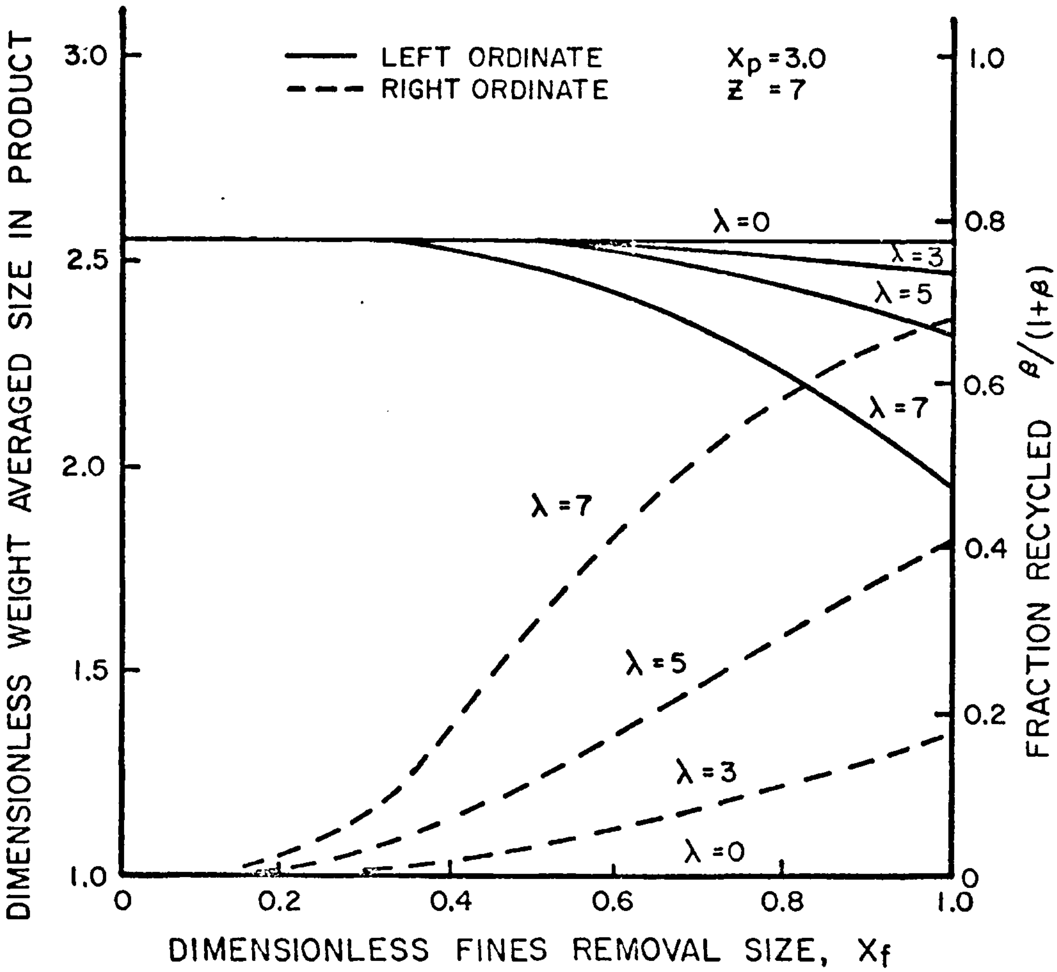


Fig. 21. Effect of Fines Removal Parameters on Product Average Size and Fraction of Internal Production Recycled.

For the case of classified product removal only with $z = 5$ and $L_p = 300$ microns, the solution of Eq. (8) yields $G_0 = 3.0$ µm/min. Thus $x_p$ is found to be 5.0. Checking Figure 11, the stability limit is found to be at $i = 12$; therefore the system would be expected to be stable. The dynamics of this system to a step change are presented by Nuttall (1971, p. 120) and display a stable nature.

When fines removal is added to increase the average size of product and narrow the CSD, the growth rate must increase. Solving Eq. (8) with the addition of $R = 5$ and $L_f = 100$ µm, $G_0$ is found to be close to 5.0 µm/min. The new dimensionless parameters are $x_f = 1.0$, $\lambda = 4.0$, $z = 5.0$, and $x_p = 3.0$. The weight-averaged size of product was raised from 210 µm to 240 µm by removing fines. First, consider the case involving no recycle of fines. From Figure 8 complete stabilization of CSD would be expected owing to the size of $x_f$. Figure 22 gives the dynamics of this situation in terms of the normalized third moment $f_3$. The system reaches the new steady state twice as fast as in the purely classified example. If fines are recycled, then the system may be unstable for the kinetic order of six used for the simulation since the product average size is 80% of the classification size. The value of i found as the limit of stability was 5.9; therefore the recycle case would be predicted to be cyclic. The cyclic nature of the simulated CSD dynamics is presented in terms of $f_3$ in Figure 22. Cycling was unabated after solution of the nonlinear equations for 15 residence times of the crystallizer. The above examples illustrate the validity of the linearized R-z model stability boundaries through the solution of the complete, nonlinear model.

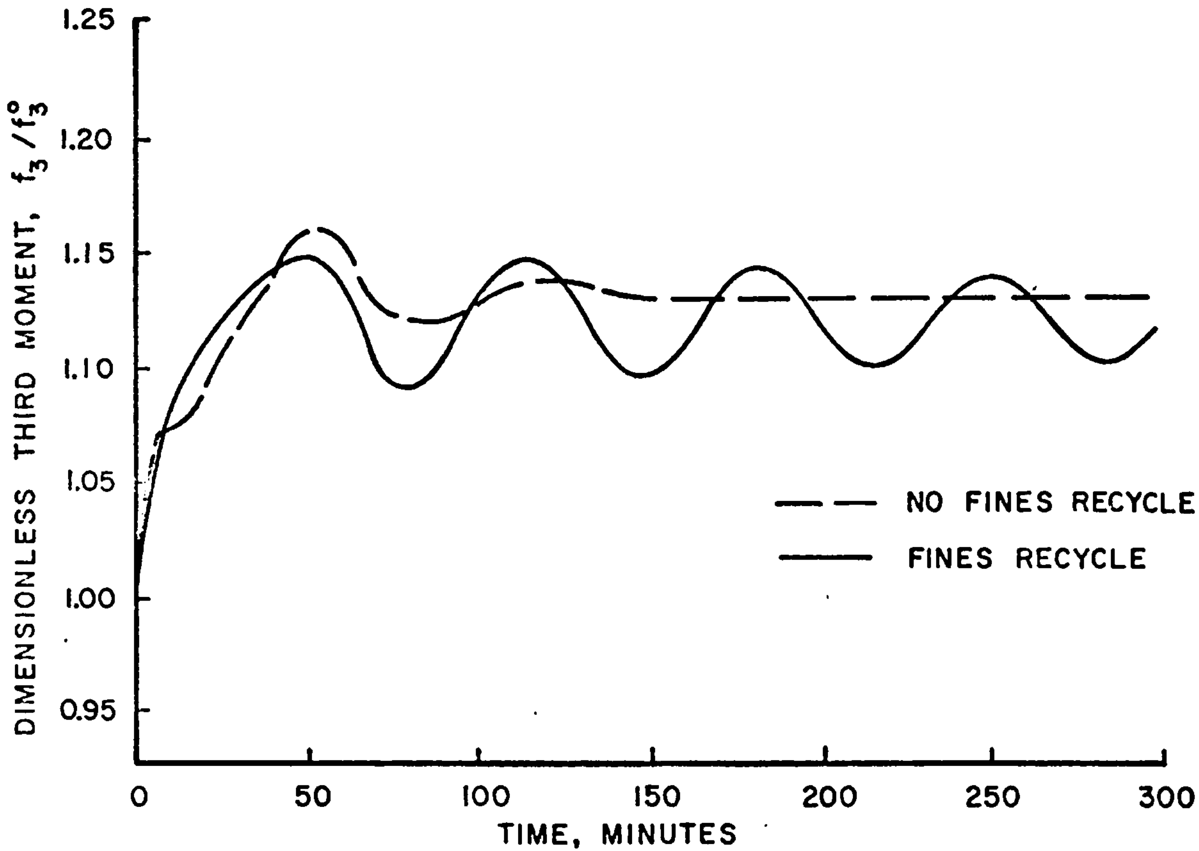


Fig. 22. Response of the Third Moment of CSD to Step Change in Solute Resources for the Classified Crystallizer with Fines Destruction.

## DISCUSSION OF RESULTS

The appearance of low-order CSD cycling can be explained by the destabilizing effects of fines removal (with dissolved mass recycle) combined with product classification. These two configurational influences work in concert to lower the stability limit, i, for the R-z crystallizer model to realistic values in the range from one to three as observed in MSMPR nucleation kinetics studies. Classification is the *sine qua non* of configurationally-induced cyclic behavior and accomplishes most of the destabilization. Fines destruction with recycle interacts with classification to bring the sensitivity threshold down the last step into low-order levels.

Fines removal, even when accompanied by internal recycle of the destroyed fines mass, can also stabilize CSD. As the maximum size of fines removed is increased at constant survival probability $e^{-\lambda}$, a point is eventually reached beyond which the system becomes more and more stable. This effect of fines removal may offer the best solution to eliminating CSD cycling. If product size is to be maintained, then $\lambda$ must be held at a constant value. The removal rate (R-1) and maximum fines size $x_f$ can be adjusted simultaneously to set $\lambda = (R-1)x_f$ at nearly the same level, while increasing $x_f$ into a stable region. The other alternative, again with the aim of preserving the desired product CSD, would involve an external recycle of fines to a holding tank and subsequent reuse at feed concentration. The large flow rate of fluid would tend to make this procedure impractical unless the fines could be concentrated at removal.

In analyzing CSD stability using the Class II R-z model, the steady-state calculation for growth rate must be made in order to determine the dimensionless sizes used in the analysis. Ratios of these sizes, however, eliminate dependence on a steady-state growth rate. Subsequently, certain factors such as the relative size of product to the size of classification (for $\beta/(1+\beta)$ less than 0.3) may be examined, at least for estimation purposes without recourse to the steady-state growth rate iteration.

Conditions resulting in unstable behavior as predicted by the linearized analysis should also result in sustained limit cycles of nonlinear solutions of the R-z model equations since constrained physical systems cannot violate certain boundaries (mass balances and other essentially nonlinear limits). Instabilities in a linear region near a steady state will drive the solution toward one of these boundaries. The nonlinearities then return it to the linear region and the cycle is perpetuated. This limit cycle behavior was observed in the rigorous numerical solutions of Nuttall for unstable conditions predicted with the present linearized stability analysis.

# CONCLUSIONS

1. Recycle of dissolved fines lowers stability limits for CSD.

2. Fines removal alone, even with internal recycle, cannot account for low-order cycling of CSD.

3. Classification at product sizes lower than $4G_0\tau$ significantly destabilizes CSD.

4. Classified removal rates greater than 7 times the mixed removal rate ($z = 7$) do not further contribute to CSD instability.

5. Low-order CSD cycling can be predicted by combined classification and fines recycle with the R-z crystallizer model.

6. Externalization of fines recycle or the increasing of fines removal size can be used to stabilize CSD.

7. Magma-density-dependent nucleation tends to stabilize CSD, but this effect is slight.

8. Specific systems display their individuality through the steady-state calculations producing $G_0$; calculation of $G_0$ using the steady-state R-z algorithm is the first step in analyzing crystallizer stability.

# RECOMMENDATIONS FOR FUTURE WORK

The construction of a laboratory scale Class II cyclic crystallizer should be possible using the stability information contained here. The system should be one of good crystal habit and possessing a kinetic order above 2 to ease the amount of classification and fines recycle necessary to produce cycling. A salting out system such as ammonium sulfate-ethanol-water or an inorganic salt-water system could be used. The holding time would have to be short enough to allow 15 or more residence times to be completed in a run. A holding time of 30 minutes with a crystallizer volume of 5 liters might be reasonable if the entire system were made semicontinuous by eventually converting all crystal product into uniform feed solution though this would be difficult in a salting out system. If a solids concentration of 0.15 g/cm$^3$ were assumed, then fines could be destroyed and recycled at sizes below 50 μm and classification could be commenced near 200 μm. The small sizes involved could lead to problems of design for the fines removal and classifying devices, but the difficulties should not be insurmountable. Simulation of the system would aid in design as well as in parameter selection. The key would be to classify strongly enough at an acceptably small size while removing fines at as small a maximum size and as high a rate as possible.

## APPENDIX A

## DEVELOPMENT OF STEADY-STATE GROWTH RATE

The external production rate for a Class II system may be written as (Randolph and Larson 1971, p. 145)

$$P_E = 6\rho k_V n_0{}^0 (G_0\tau)^4 D_p Q. \tag{A-1}$$

Next, assume a steady-state nucleation rate of

$$B_0{}^0/G_0 = n_0{}^0 = k_N G_0^{i-1} M_{T0}^{j} . \tag{A-2}$$

The expression for solids concentration in a Class II R-z crystallizer is given as

$$M_{T0} = \rho k_V \int_0^\infty n\, L^3\, dL = \rho k_V (G_0\tau)^4 n_0{}^0 6D. \tag{A-3}$$

Now if the solids concentration expression is brought to the nucleation Eq. (A-2), we have

$$n_0{}^0 = k_N G^{\,i-1} \left[\rho k_V (G_0\tau)^4 n_0{}^0 6D\right]^j \tag{A-4}$$

or

$$n_0{}^0 = k_N^{\frac{1}{1-j}}\, G_0^{\frac{i-1+4j}{1-j}}\, (\rho k_V 6D)^{\frac{j}{1-j}}\, \tau^{\frac{4j}{1-j}} . \tag{A-5}$$

Combining Eq. (A-5) with the external production relationship given in Eq. (A-1) results in

$$P_E = 6\, k_N^{\frac{1}{1-j}} (\rho k_V)^{\frac{1}{1-j}}\, \tau^{\frac{4}{1-j}}\, (6D)^{\frac{j}{1-j}}\, D_p\, Q\, G_0^{\frac{i+3}{1-j}} . \tag{A-6}$$

Solving the production expression of Eq. (A-6) for $G_0$ yields

$$G_0 = \left(\frac{P_E}{6D_pQ}\right)^{\frac{1-j}{i+3}} k_N^{-\frac{1}{i+3}} (\rho k_V)^{-\frac{1}{i+3}} \tau^{-\frac{4}{i+3}} (6D)^{-\frac{j}{i+3}} \tag{A-7}$$

or

$$G_0 = \left(\frac{P_E}{6D_pQ}\right)^{\frac{1-j}{i+3}} (k_N \rho k_V \tau^4)^{-\frac{1}{i+3}} (6D)^{-\frac{j}{i+3}} , \tag{A-8}$$

which is the implicit equation for the generalized R-z model steady-state growth rate. When the kinetic parameter j is equal to unity, growth rate is independent of production rate.

## APPENDIX B

## MASS BALANCE DERIVATION

Using the solute balances and material balance given by Hulbert and Katz (1964), Nuttall (1971, p. 69) derives the following dynamic concentration balance

$$\frac{Q\varepsilon_i}{V}(C_i - C) + (3k_V\int_0^\infty GnL^2dL)(C - \rho) = \varepsilon\frac{dC}{dt}. \tag{B-1}$$

If we now take the limit of Class II behavior ($C \to C_s$) with growth rate not a function of size and with clear liquor feed ($\varepsilon_i = 1$), the balance becomes

$$\frac{Q}{V}(C_i - C_s) + 3k_VG(C_s - \rho)\int_0^\infty n\,L^2\,dL = 0. \tag{B-2}$$

Solving Eq. (B-2) for G produces

$$G = \frac{Q\left(\dfrac{C_s - C_i}{C_s - \rho}\right)}{3k_VV\displaystyle\int_0^\infty nL^2dL}. \tag{B-3}$$

Now if we use the fact that $k_a = 6k_V$ and if we convert from the slurry basis to a clear liquor basis, we obtain

$$G = \frac{P_I}{\dfrac{\rho V}{2}(k_a\displaystyle\int_0^\infty nL^2dL)} = \frac{P_I}{\dfrac{\rho V}{2}A}, \tag{B-4}$$

which is identical to the relationship derived as an internal solute balance, given by Eq. (16) in the text.

## APPENDIX C

## LINEARIZATION OF THE MODEL

The nonlinear set of equations for the R-z model can be stated as

$$\frac{\partial y}{\partial \theta} + \phi \frac{\partial y}{\partial x} + hy = 0 \tag{C-1}$$

$$\phi = (1 + \beta f_{3,1}) / [(1 + \beta) f_2]$$

$$y(x,0) = \overline{y}, \qquad y(0,\theta) = f_3{}^j \phi^{i-1}.$$

We make perturbations about a steady state through

$$y(x,\theta) = \overline{y}(x) + \tilde{y}(x,\theta) \tag{C-2}$$

$$\phi = \overline{\Phi} + \tilde{\phi} = 1 + \tilde{\phi}$$

$$f_i = 1 + \tilde{f}_i.$$

After incorporation into the population balance contained in Eq. (C-1), we have

$$\frac{\partial \tilde{y}}{\partial \theta} + \frac{\partial \tilde{y}}{\partial x} + \frac{\partial \overline{y}}{\partial x} (1 + \tilde{\phi}) + h(\overline{y} + \tilde{y}) = 0, \tag{C-3}$$

which can be expanded as

$$\frac{\partial \tilde{y}}{\partial \theta} + \frac{\partial \tilde{y}}{\partial x} + \tilde{\phi} \frac{\partial \tilde{y}}{\partial x} + \frac{d\overline{y}}{dx} + \tilde{\phi} \frac{d\overline{y}}{dx} + h\overline{y} + h\tilde{y} = 0. \tag{C-4}$$

Now $\tilde{\phi}(\partial\tilde{y}/\partial x)$ is a second-order perturbation, and $d\bar{y}/dx + h\bar{y} = 0$ is the steady-state solution. Therefore, the linearized population balance reduces to

$$\frac{\partial\tilde{y}}{\partial\theta} + \frac{\partial\tilde{y}}{\partial x} + \tilde{\phi}\frac{d\bar{y}}{dx} + h\tilde{y} = \frac{\partial\tilde{y}}{\partial\theta} + \frac{\partial\tilde{y}}{\partial x} + \tilde{\phi}h\bar{y} + h\tilde{y} = 0. \qquad \text{(C-5)}$$

The mass balance part of Eq. (C-1) may be expanded as

$$\phi = 1 + \tilde{\phi} = \frac{1 + \beta(1 + \tilde{f}_{3,1})}{1 + \beta} \cdot \frac{1}{1 + \tilde{f}_2} \qquad \text{(C-6)}$$

or

$$(1 + \tilde{\phi})(1 + \tilde{f}_2) = 1 + \left(\frac{\beta}{1 + \beta}\right)\tilde{f}_{3,1}\ . \qquad \text{(C-7)}$$

Expanding the equation and dropping higher-order terms yields

$$1 + \tilde{\phi} + \tilde{f}_2 = 1 + \left(\frac{\beta}{1 + \beta}\right)\tilde{f}_{3,1}\ . \qquad \text{(C-8)}$$

Solving for $\tilde{\phi}$ finally gives

$$\tilde{\phi} = \left(\frac{\beta}{1 + \beta}\right)\tilde{f}_{3,1} - \tilde{f}_2 \qquad \text{(C-9)}$$

as the linearized mass balance.

Considering the nucleation-rate-containing equation in Eq. (C-1) we have

$$1 + \tilde{y}(0,\theta) = 1 + j\tilde{f}_3 + (i-1)\tilde{\phi} \qquad \text{(C-10)}$$

or

$$\tilde{y}(0,\theta) = j\tilde{f}_3 + (i-1)\tilde{\phi}. \qquad \text{(C-11)}$$

The initial condition is

$$\tilde{y}(x,0) = 0. \tag{C-12}$$

The complete linearized set, after inclusion of $\tilde{\phi}$ into the various expressions, is

$$\frac{\partial\tilde{y}}{\partial\theta} + \frac{\partial\tilde{y}}{\partial x} + h\bar{y}\tilde{f}_2 - \left(\frac{\beta}{1+\beta}\right)\tilde{f}_{3,1} + h\tilde{y} = 0 \tag{C-13}$$

$$\tilde{y}(x,0) = 0$$

$$\tilde{y}(\theta,0) = j\tilde{f}_3 + \frac{(i-1)\beta}{1+\beta}\tilde{f}_{3,1} - (i-1)\tilde{f}_2.$$

## APPENDIX D

## SPECTRAL ANALYSIS

Given a linear partial differential equation of the form

$$\frac{\partial \tilde{y}}{\partial \theta} - \frac{\beta}{1+\beta} h\bar{y}\tilde{f}_{3,1} + h\bar{y}\tilde{f}_2 + \frac{\partial \tilde{y}}{\partial x} + h\tilde{y} = 0 \tag{D-1}$$

with end condition

$$\tilde{y}(\theta,0) = j\tilde{f}_3 + (i-1)\frac{\beta}{1+\beta}\tilde{f}_{3,1} - (i-1)\tilde{f}_2. \tag{D-2}$$

Now assume a solution of the form

$$\tilde{y} = e^{-s\theta}U(x) \tag{D-3}$$

and define the values of the integral ratio $F_2$, $F_3$, and $F_{3,1}$ as (all constants for continuous $U(x)$)

$$\tilde{f}_2 = e^{-s\theta}\int_0^\infty U(x)\,x^2\,dx \Big/ \int_0^\infty x^2\,\bar{y}\,dx = e^{-s\theta}F_2 \tag{D-4}$$

$$\tilde{f}_3 = e^{-s\theta}F_3$$

$$\tilde{f}_{3,1} = e^{-s\theta}F_{3,1}.$$

Making the above substitutions, the equation and end condition become

$$se^{-\theta s}U(x) - \left(\frac{\beta}{1+\beta}\right)h\,\bar{y}\,e^{-\theta s}F_{3,1} + h\,\bar{y}\,F_2\,e^{-\theta s} + e^{-\theta s}\frac{dU(x)}{dx} + he^{-\theta s}U(x) = 0 \tag{D-5}$$

$$e^{-\theta s}U(0) \quad = \quad jF_3e^{-\theta s} + \frac{(i-1)\beta}{1+\beta} F_{3,1}e^{-\theta s} - (i-1)F_2e^{-\theta s} \ .$$

Canceling $e^{-\theta s}$ throughout, we attain

$$\frac{dU(x)}{dx} + (h-s)U(x) \quad = \quad \left(\frac{\beta}{1+\beta} F_{3,1} - F_2\right) h\,\overline{y}$$

$$U(0) \quad = \quad jF_3 + \frac{(i-1)\beta}{1+\beta} F_{3,1} - (i-1)F_2 \ . \tag{D-6}$$

Solving this first-order ordinary differential equation using an integrating factor, we arrive at

$$U(x) = \exp\left(-\int (h-s)dx\right) \cdot \left[\int \exp\left(\int (h-s)dx\right) \cdot \left(\frac{\beta}{1+\beta} F_{3,1} - F_2\right) h\,\overline{y}\,dx + C_I\right] \ . \tag{D-7}$$

Using the following simplifications

$$H(x) \quad = \quad \exp\left[sx - \int_0^\infty h(\tau)d\tau\right]$$

$$G(x) \quad = \quad \int_0^\infty he^{-sx}dx \tag{D-8}$$

$$\overline{y} \quad = \quad \exp\left[-\int_0^\infty h(\tau)d\tau\right]$$

so that the solution may be written

$$U(x) \quad = \quad C_IH(x) + \left(\frac{\beta}{1+\beta} F_{3,1} - F_2\right) G(x)\,H(x) \tag{D-9}$$

and applying the end condition to eliminate the constant of integration, we find

$$U(x) = \left[jF_3 + \frac{(i-1)\beta}{1+\beta} F_{3,1} - (i-1)F_2\right]H(x) + \left(\frac{\beta}{1+\beta} F_{3,1} - F_2\right)H(x)G(x) \ . \tag{D-10}$$

To obtain from the arbitrary function U(x) the constants $F_2$, $F_3$ and $F_{3,1}$, the implicit solution above may be multiplied by $x^2dx$, $x^3dx$, and $x^3dx$, then integrated over the limits $0 \to \infty$, $0 \to \infty$, $0 \to x_f$, respectively. This removes the function U(x) from consideration and produces the explicit set

$$Y_\infty^2 F_2 = \left[ jF_3 + \frac{(i-1)\beta}{1+\beta} F_{3,1} - (i-1)F_2 \right] H_\infty^2 + \left( \frac{\beta}{1+\beta} F_{3,1} - F_2 \right) G_\infty^2$$

$$Y_\infty^3 F_3 = \left[ jF_3 + \frac{(i-1)\beta}{1+\beta} F_{3,1} - (i-1)F_2 \right] H_\infty^3 + \left( \frac{\beta}{1+\beta} F_{3,1} - F_2 \right) G_\infty^3$$

$$Y_{x_f}^3 F_{3,1} = \left[ jF_3 + \frac{(i-1)\beta}{1+\beta} F_{3,1} - (i-1)F_2 \right] H_{x_f}^3 + \left( \frac{\beta}{1+\beta} F_{3,1} - F_2 \right) G_{x_f}^3 . \tag{D-11}$$

The matrix equation shown in Figure 6 may be found directly from Eq. (D-11). The parameters used in Eq. (D-11) are

$$H_\alpha^k = \int_0^\alpha x^k H(x)\, dx$$

$$G_\alpha^k = \int_0^\infty x^k G(x)\, H(x)\, dx \tag{D-12}$$

$$Y_\alpha^k = \int_0^\infty x^k \, \overline{y}\, dx .$$

In order to write the matrix equation, and thus the characteristic equation, in terms of the model variables R, z, $x_f$, $x_p$ and in terms of the spectral variable s, the functions must be expanded as continuous functions of x. Writing out these basic relations yields

$$h = \begin{cases} R, & 0 \le x \le x_f \\ 1, & x_f \le x \le x_p \\ z, & x_p \le x \end{cases} \tag{D-13}$$

$$\int_0^x h(\tau)\,d\tau = \begin{cases} Rx, & 0 \le x \le x_f \\ (R-1)x_f + x, & x_f \le x \le x_p \\ (R-1)x_f + (1-z)x_p + zx, & x_p \le x \end{cases} \qquad \text{(D-14)}$$

$$H(x) = \begin{cases} \exp\left[(s-R)x\right], & 0 \le x \le x_f \\ \exp\left[-(R-1)x_f + (s-1)x\right], & x_f \le x \le x_p \\ \exp\left[-(R-1)x_f + (1-z)x_p + (s-z)x\right], & x_p \le x \end{cases} \qquad \text{(D-15)}$$

$$G(x) = \begin{cases} \frac{R}{s}\left[1 - \exp(-sx)\right], & 0 \le x \le x_f \\ \frac{1}{s}\left[R + (1-R)\exp(-sx_f)\right] - \frac{1}{s}\exp(-sx), & x_f \le x \le x_p \\ \frac{1}{s}\left[R + (1-R)\exp(-sx_f) + (z-1)\exp(-sx_p)\right], & x_p \le x \end{cases} \qquad \text{(D-16)}$$

$$\overline{y} = \begin{cases} \exp(-Rx), & 0 \le x \le x_f \\ \exp\left[-(R-1)x_f - x\right], & x_f \le x \le x_p \\ \exp\left[-(R-1)x_f + (1-z)x_p - zx\right], & x_p \le x\,. \end{cases} \qquad \text{(D-17)}$$

So, for $k = 2,3$,

$$H_\infty^k = \int_0^{x_f} x^k H(x)\,dx + \int_{x_f}^{x_p} x^k H(x)\,dx + \int_{x_p}^{\infty} H(x)\,dx \qquad \text{(D-18)}$$

or

$$H_\infty^k = \int_0^{x_f} x^k e^{(s-R)x}\,dx + e^{-(R-1)x_f}\int_{x_f}^{x_p} x^k e^{(s-1)x}\,dx$$

$$+ e^{-\left[(R-1)x_f + (1-z)x_p\right]}\int_{x_p}^{\infty} x^k e^{(s-z)}\,dx\,. \qquad \text{(D-19)}$$

Introducing the notational conventions

$$
\begin{aligned}
E_1 &= 1.0 \\
E_2 &= \exp\left[-(R-1)x_f\right] \\
E_3 &= \exp\left[-(R-1)x_f + (1-z)x_p\right]
\end{aligned}
\tag{D-20}
$$

and

$$
I_2(s,\nu,\gamma) = \frac{\exp[(s-\nu)\gamma]}{(s-\nu)^3}\left[(s-\nu)^2\gamma^2 - 2(s-\nu)\gamma + 2\right] \tag{D-21}
$$

$$
I_3(s,\nu,\gamma) = \frac{\exp[(s-\nu)\gamma]}{(s-\nu)^4}\left[(s-\nu)^3\gamma^3 - 3(s-\nu)^2\gamma^2 + 6(s-\nu)\gamma - 6\right],
$$

we see that

$$
\begin{aligned}
H_{x_f}{}^3 &= E_1\left[I_3(s,R,x_f) - I_3(s,R,0)\right] \\
H_\infty{}^2 &= E_1\left[I_2(s,R,x_f) - I_2(s,R,0)\right] + E_2\left[I_2(s,1,x_p) - I_2(s,1,x_f)\right] \\
&\quad + E_3\left[-I_2(s,z,x_p)\right] \\
H_\infty{}^3 &= E_1\left[I_3(s,R,x_f) - I_3(s,R,0)\right] + E_2\left[I_3(s,1,x_p) - I_3(s,1,x_f)\right] \\
&\quad + E_3\left[-I_3(s,z,x_p)\right].
\end{aligned}
\tag{D-22}
$$

Now, to find $G_\alpha^k$, we first write

$$
G(x)\,H(x) = \begin{cases}
\frac{R}{s}\left[e^{(s-R)x} - \bar{y}\right], & 0 \le x \le x_f \\[2ex]
\frac{e^{-(R-1)x_f}}{s}\left[R + (1-R)e^{-sx_f}\right]e^{(s-1)x} - \frac{1}{s}\,\bar{y}, & x_f \le x \le x_p \\[2ex]
\frac{e^{-[(R-1)x_f + (1-z)x_p]}}{s}\left[R + (1-R)e^{-sx_f} + (z-1)e^{-sx_p}\right] \\
\quad \cdot\, e^{(s-z)x_p} - (z/s)\bar{y}, & x_p \le x.
\end{cases}
\tag{D-23}
$$

Then from the definition of $G_\alpha^k$ we have

$$G_\infty^k = \int_0^{x_f} x^k G(x)H(x)\,dx + \int_{x_f}^{x_p} x^k G(x)H(x)\,dx + \int_{x_p}^{\infty} x^k G(x)H(x)\,dx \tag{D-24}$$

or

$$\begin{aligned} G_\infty^k = {} & \frac{R}{s}\int_0^{x_f} x^k\, e^{(s-R)x}dx + \frac{e^{-(R-1)x_f}}{s}\left[R + (1-R)e^{-sx_f}\right]\int_{x_f}^{x_p} x^k e^{(s-1)x}dx \\ & + e^{-\left[(R-1)x_f + (1-z)x_p\right]}\left[R + (1-R)e^{-sx_f} + (z-1)e^{-sx_f}\right] \\ & \cdot \int_{x_p}^{\infty} x^k e^{(s-z)x}dx \\ & - \frac{R}{s}\int_0^{x_f} \bar{y}\, x^k\,dx \; - \frac{1}{s}\int_{x_f}^{x_p} \bar{y}\, x^k\,dx \; - \frac{z}{s}\int_{x_p}^{\infty} \bar{y}\, x^k\,dx. \end{aligned} \tag{D-25}$$

Using the previous notation with the addition of

$$\begin{aligned} A_1 &= R/s \\ A_2 &= R/s - \left[(R-1)/s\right]e^{-sx_f} \\ A_3 &= R/s - \left[(R-1)/s\right]e^{-sx_f} + \frac{z-1}{s}e^{-sx_p} \end{aligned} \tag{D-26}$$

$$\begin{aligned} m_{k,1}^{o} &= \int_0^{x_f} x^k\,\bar{y}\,dx \\ m_{k,2}^{o} &= \int_{x_f}^{x_p} x^k\,\bar{y}\,dx \\ m_{k,3}^{o} &= \int_{x_p}^{\infty} x^k\,\bar{y}\,dx \end{aligned} \tag{D-27}$$

the final expression of $G_\alpha^k$ becomes

$$G_{x_f}{}^3 = A_1E_1\left[I_3(s,R,x_f) - I_3(s,R,0)\right] - (R/s)m_{3,1}^{o}$$

$$\begin{aligned} G_\infty{}^2 = {} & A_1E_1\left[I_2(s,R,x_f) - I_2(s,R,0)\right] \\ & + A_2E_2\left[I_2(s,1,x_p) - I_2(s,1,x_f)\right] + A_3E_3\left[-I_2(s,z,x_p)\right] \\ & - (R/s)m_{2,1}^{o} - (1/s)m_{2,2}^{o} - (z/s)m_{2,3}^{o} \end{aligned}$$

$$\begin{aligned} G_\infty{}^3 = {} & A_1E_1\left[I_3(s,R,x_f) - I_3(s,R,0)\right] \\ & + A_2E_2\left[I_3(s,1,x_p) - I_3(s,1,x_f)\right] + A_3E_3\left[-I_3(s,z,x_p)\right] \\ & - (R/s)m_{3,1}^{o} - (1/s)m_{3,2}^{o} - (z/s)m_{3,3}^{o} \,. \end{aligned} \tag{D-28}$$

The simplified expression for $Y_\alpha^k$ is

$$Y_{x_f}{}^3 = m_{3,1}^{o}$$

$$Y_\infty{}^2 = m_{2,1}^{o} + m_{2,2}^{o} + m_{2,3}^{o}$$

$$Y_\infty{}^3 = m_{3,1}^{o} + m_{3,2}^{o} + m_{3,3}^{o} \,. \tag{D-29}$$

Equations (D-22), (D-28), and (D-29) together with (D-11) complete the linearized, spectral description in the framework of the R-z model.

## APPENDIX E

## EXPANSION OF THE CHARACTERISTIC DETERMINANT

The expression det(A) = 0 represents the characteristic equation. To obtain an algebraic equation, the determinant must be expanded. The det(A) is

$$\begin{vmatrix} (i-1)H_\infty^2 + G_\infty^2 + Y_\infty^2 & jH_\infty^2 & \frac{(i-1)\beta}{1+\beta} H_\infty^2 + \frac{\beta}{1+\beta} G_\infty^2 \\ (i-1)H_\infty^3 + G_\infty^3 & jH_\infty^3 - Y_\infty^3 & \frac{(i-1)\beta}{1+\beta} H_\infty^3 + \frac{\beta}{1+\beta} G_\infty^3 \\ (i-1)H_{xf}^3 + G_{xf}^3 & jH_{xf}^3 & \frac{(i-1)\beta}{1+\beta} H_{xf}^3 + \frac{\beta}{1+\beta} G_{xf}^3 - Y_{xf}^3 \end{vmatrix} . \tag{E-1}$$

Expanding by minors about the second column yields the terms

$$-jH_\infty^2 \Big\{ \left[(i-1)H_\infty^3 + G_\infty^3\right]\left[\frac{(i-1)\beta}{1+\beta} H_{xf}^3 + \frac{\beta}{1+\beta} G_{xf}^3 - Y_{xf}^3\right] - \left[(i-1)H_{xf}^3 + G_{xf}^3\right]\left[\frac{(i-1)\beta}{1+\beta} H_\infty^3 + \frac{\beta}{1+\beta} G_\infty^3\right]\Big\} \tag{E-2}$$

$$(jH_\infty^3 - Y_\infty^3) \Big\{ \left[(i-1)H_\infty^2 + G_\infty^2 + Y_\infty^2\right]\left[\frac{(i-1)\beta}{1+\beta} H_{xf}^3 + \frac{\beta}{1+\beta} G_{xf}^3 - Y_{xf}^3\right] - \left[(i-1)H_{xf}^3 + G_{xf}^3\right]\left[\frac{(i-1)\beta}{1+\beta} H_\infty^2 + \frac{\beta}{1+\beta} G_\infty^2\right]\Big\} \tag{E-3}$$

$$-jH_{xf}^3 \Big\{ \left[(i-1)H_\infty^2 + G_\infty^2 + Y_\infty^2\right]\left[\frac{(i-1)\beta}{1+\beta} H_\infty^3 + \frac{\beta}{1+\beta} G_\infty^3\right] - \left[(i-1)H_\infty^3 + G_\infty^3\right]\left[\frac{(i-1)\beta}{1+\beta} H_\infty^2 + \frac{\beta}{1+\beta} G_\infty^2\right]\Big\} \tag{E-4}$$

with the sum of expressions (E-2), (E-3), and (E-4) being the algebraic form of the characteristic equation. Now if we write out the terms containing the highest order of i (omitting (i-1) as a factor), we obtain from expression (E-2)

$$-j \frac{\beta}{1+\beta} H_\infty^2 H_\infty^3 H_{x_f}^3 + j \frac{\beta}{1+\beta} H_\infty^2 H_\infty^3 H_{x_f}^3 = 0, \tag{E-5}$$

from expression (E-3)

$$(jH_\infty^3 - Y_\infty^3)\left( \frac{\beta}{1+\beta} H_\infty^2 H_{x_f}^3 - \frac{\beta}{1+\beta} H_\infty^2 H_{x_f}^3 \right) = 0, \tag{E-6}$$

and from expression (E-4)

$$-jH_{x_f}^3\left( \frac{\beta}{1+\beta} H_\infty^2 H_\infty^3 - \frac{\beta}{1+\beta} H_\infty^2 H_\infty^3 \right) = 0. \tag{E-7}$$

Therefore the characteristic equation is at most linear in (i-1). Writing out the terms in (i-1) and canceling a great many of them produces

$$T_1(i-1) = (Y_\infty^3 H_\infty^2 Y_{x_f}^3 - Y_\infty^3 Y_\infty^2 H_{x_f}^3 \frac{\beta}{1+\beta})(i-1). \tag{E-8}$$

Collecting the terms not containing (i-1), we have

$$\begin{aligned} T_2 = {} & j(H_\infty^2 G_\infty^3 Y_{x_f}^3 - H_\infty^3 G_\infty^2 Y_{x_f}^3 - H_\infty^3 Y_\infty^2 Y_{x_f}^3) \\ & - \frac{\beta}{1+\beta} Y_\infty^3 Y_\infty^2 G_{x_f}^3 + Y_\infty^3 G_\infty^2 Y_{x_f}^3 + Y_\infty^3 Y_\infty^2 Y_{x_f}^3 \\ & + j \frac{\beta}{1+\beta} (H_\infty^3 Y_\infty^3 G_{x_f}^3 - Y_\infty^2 G_\infty^3 H_{x_f}^3). \end{aligned} \tag{E-9}$$

Thus the characteristic equation may be written as

$$T_1(i-1) + T_2 = 0 \tag{E-10}$$

or

$$(i-1) = -T_2/T_1 = \psi(s). \tag{E-11}$$

## NOMENCLATURE

| | |
|---|---|
| $A(t)$ | Crystal area in suspension |
| $b$ | Search variable lm(s) = b |
| $B^0$, $B_0{}^0$ | Nucleation rate |
| $\mathcal{B}$ | Birth function (Randolph 1964) |
| $C$ | Concentration in crystallizer |
| $C_i$ | Concentration in feed |
| $C_s$ | Saturation concentration |
| CSD | Crystal size distribution |
| $D$, $D_p$ | Dimensionless functions in steady-state growth rate equation |
| $\mathcal{D}$ | Death function (Randolph 1964) |
| $f_{j,K}$ | Dimensionless normalized moments of distributed growth rate equation |
| $G$, $G_0$ | Dynamic and steady-state growth rates |
| $G(x)$, $G_\alpha^n$ | Integral functions used in spectral analysis |
| $h(L)$, $h(x)$ | Removal function |
| $H(x)$, $H_\alpha^n$ | Integral functions used in spectral analysis |
| $i$ | Nucleation/growth rate kinetic sensitivity parameter |
| $j$ | Magma-dependent nucleation kinetics exponent |
| $k_a$ | Shape factor for area |
| $k_N$ | Nucleation constant |
| $k_V$ | Shape factor for volume |
| $L$ | Characteristic particle size |
| $L_f$ | Particle size at upper limit of fines destruction |

| | |
|---|---|
| $L_p$ | Particle size at lower limit of classification |
| MSMPR | Mixed suspension mixed product removal |
| $M_T$ | Solids concentration |
| $n(L,t)$, $n_0(L)$ | Dynamic and steady-state number density function |
| $n^0$, $n_0^0$ | Dynamic and steady-state nuclei density |
| $P_I$ | Internal production rate |
| $P_E$ | External production rate |
| Q | Flow rate through crystallizer |
| R | Ratio of total fines removal rate (product plus fines trap) to flow through crystallizer |
| s | Spectral variable |
| t | Time |
| V | Crystallizer volume |
| x | Dimensionless particle size |
| $x_f$, $x_p$ | Dimensionless size limits for fines removal or classification |
| $\overline{X}_{prod}$ | Average size in product |
| y | Dimensionless number density |
| $\overline{y}$ | Steady-state dimensionless number density |
| $y^0$ | Dimensionless nuclei density |
| $y^n$ | Integral over $\overline{y}$ used in spectral analysis |
| $Y(x)$, $Y_\alpha^n$ | Integral functions used in spectral analysis |
| z | Ratio of classified product removal to flow through crystallizer |
| $\alpha$ | Upper limit of integral functions |
| $\beta$ | Ratio of fines destruction to external production |
| $\varepsilon$ | Void fraction |

| | |
|---|---|
| $\theta$ | Dimensionless time |
| $\lambda$ | Dissolving parameter, $(R-1)x_f$ |
| $\rho$ | Crystal density |
| $\tau$ | Residence time based on mixed removal rate |
| $\phi$ | Dimensionless growth rate |
| $\psi$ | Characteristic equation functional |
| $\nabla$ | Differential operator |
| $\sim$ | (Superscript) Linearized form of variable |

## LITERATURE CITED


Hulburt, H. M., and Katz, S. "Some Problems in Particle Technology," Chem. Engr. Sci., 19;555 (1964).

Hulburt, H. M., and Stefango, D. G. "Design Models for Continuous Crystallizers with Double Draw-Off," Chem. Engr. Prog. Sym. Ser. No. 95, 65;50 (1969).

Lei, S. J., Shinnar, R., and Katz, S. "The Stability and Dynamics of a Continuous Crystallizer with Fines Trap," AIChE J., 17;1459 (1971a).

Lei, S. J., Shinnar, R., and Katz, S. "Feedback Control of a Continuous Crystallizer with and without Fines Trap," Chem. Engr. Prog. Sym. Ser. No. 110, 67;129 (1971b).

Nuttall, H. E. "Computer Simulation of Steady-State and Dynamic Crystallizers," Ph.D. Dissertation, University of Arizona, Tucson, Arizona, 1971.

Randolph, A. D. "A Population Balance for Countable Entities," Can. J. Chem. Engr., 42;280 (1964).

Randolph, A. D. "Comments on Recent Advances in the Analysis of Crystallization Processes," Chem. Engr. Prog. Sym. Ser. No. 115, 65;2 (1971).

Randolph, A. D., and Cise, M. D. "Nucleation Kinetics of Potassium Sulfate-Water System," AIChE J., 18;798 (1971).

Randolph, A. D., and Larson, M. A. Theory of Particulate Processes, Academic Press, New York, New York, 1971.

Sherwin, M., Shinnar, R., and Katz, S. "Dynamic Behavior of the Iso-Thermal Well-Mixed Crystallizer with Classified Outlet," Chem. Engr. Prog. Sym. Ser. No. 95, 65;75 (1969).

Youngquist, G. R., and Randolph, A. D. "Secondary Nucleation in a Class II System: Ammonium Sulfate-Water," AIChE J., 18;421 (1972).